5-1-2021

Molybdenite Re–Os, Titanite and Garnet U–Pb Dating of the Magushan Skarn Cu–Mo Deposit, Xuancheng District, Middle–Lower Yangtze River Metallogenic Belt

Yue Li
Hefei University of Technology

Feng Yuan
Hefei University of Technology

Simon M. Jowitt
University of Nevada, Las Vegas, simon.jowitt@unlv.edu

Fangyue Wang
Hefei University of Technology

Xiangling Li
Hefei University of Technology

Geoscience Frontiers 12 (2021) 101116

Contents lists available at ScienceDirect

Geoscience Frontiers

journal homepage: www.elsevier.com/locate/gsf

Research Paper

Molybdenite Re–Os, titanite and garnet U–Pb dating of the Magushan skarn Cu–Mo deposit, Xuancheng district, Middle–Lower Yangtze River Metallogenic Belt

Yue Li [a,b,c], Feng Yuan [a,b,*], Simon M. Jowitt [c], Fangyue Wang [a,b], Xiangling Li [a,b], Yufeng Deng [a,b], Yunyue Wang [a,b], Taofa Zhou [a,b]

[a] School of Resources and Environmental Engineering, Hefei University of Technology, Hefei 23009, China
[b] Anhui Province Engineering Research Center for Mineral Resources and Mine Environments, Hefei University of Technology, Hefei 23009, China
[c] Department of Geoscience, University of Nevada Las Vegas, 4505 S. Maryland Pkwy., NV 89154-4010, USA

ARTICLE INFO

Article history:
Received 10 July 2020
Received in revised form 12 October 2020
Accepted 26 November 2020
Available online 19 December 2020

Handling Editor: Christopher J Spencer

Keywords:
Magushan skarn deposit
Molybdenite Re–Os dating
Titanite U–Pb dating
Garnet U–Pb dating
Xuancheng ore district
Middle–Lower Yangtze River Metallogenic Belt

ABSTRACT

The Magushan skarn Cu–Mo deposit is a representative example of the skarn mineralization occurring within the Xuancheng ore district of the Middle–Lower Yangtze River Metallogenic Belt of eastern China. The precise age of an ore deposit is important for understanding the timing of mineralization relative to other geological events in a region and to fully place the formation of a mineral deposit within the geological context of other processes that occur within the study area. Here, we present new molybdenite Re–Os and titanite and andradite garnet U–Pb ages for the Magushan deposit and use these data to outline possible approaches for identifying genetic relationships in geologically complex areas. The spatial and paragenetic relationships between the intrusions, alteration, and mineralization within the study area indicates that the formation of the Magushan deposit is genetically associated with the porphyritic granodiorite. However, this is not always the case, as some areas contain complexly zoned plutons with multiple phases of intrusion or mineralization may be distal from or may not have any clear spatial relationship to a pluton. This means that it may not be possible to determine whether the mineralization formed as a result of single or multiple magmatic/hydrothermal events. As such, the approaches presented in this study provide an approach that allows the identification of any geochronological relationships between mineralization and intrusive events in areas more complex than the study area. Previously published zircon U–Pb data for the mineralization-related porphyritic granodiorite in this area yielded an age of 134.2 ± 1.2 Ma (MSWD = 1.4) whereas the Re–Os dating of molybdenite from the study area yielded an isochron age of 137.7 ± 2.5 Ma (MSWD = 0.43). The timing of the mineralizing event in the study area was further examined by the dating of magmatic accessory titanite and skarn-related andradite garnet, yielding U–Pb ages of 136.3 ± 2.5 Ma (MSWD = 3.2) and 135.9 ± 2.7 Ma (MSWD = 2.5), respectively. The dating of magmatic and hydrothermal activity within the Magushan area yields ages around 136 Ma, strongly suggesting that the mineralization in this area formed as a result of the emplacement of the intrusion. The dates presented in this study also provide the first indication of the timing of mineralization within the Xuancheng district. providing evidence of a close genetic relationship between the formation of the mineralization within the Xuancheng district and the Early Cretaceous magmatism that occurred in this area. This in turn suggests that other Early Cretaceous intrusive rocks within this region are likely to be associated with mineralization and should be considered highly prospective for future mineral exploration. This study also indicates that the dating of garnet and titanite can also provide reliable geochronological data and evidence of the timing of mineralization and magmatism, respectively, in areas lacking other dateable minerals (e.g., molybdenite) or where the relationship between mineralization and magmatism is unclear, for example in areas with multiple stages of magmatism, with complexly zoned plutons, and with distal skarn mineralization.

1. Introduction

Determining the precise timing of formation of an ore deposit is critically important for understanding the processes that formed the mineralization in an area, the geological context of a mineral deposit, and

* Corresponding author: Hefei University of Technology, Hefei 23009, China.
E-mail addresses: yueli_hfut@outlook.com (Y. Li), yf_hfut@163.com (F. Yuan), simon.jowitt@unlv.edu (S.M. Jowitt), Fywang@hfut.edu.cn (F. Wang), lixiangling_hfut@126.com (X. Li), dyfeng_214@sina.com (Y. Deng), 1785416499@163.com (Y. Wang), tfzhou@hfut.edu.cn (T. Zhou).

https://doi.org/10.1016/j.gsf.2020.11.013

determining whether hypothetical genetic relationships between ore deposits and other geological processes (e.g., igneous intrusive activity) are merely correlative or are actually causative. Establishing these relationships is particularly important for ancient ore deposits where the original textures or other key information originally preserved within the deposit or the surrounding area have most likely been deformed or overprinted by later structural, metamorphic, hydrothermal, or magmatic activities. Sulfide minerals have previously been dated using Rb–Sr and Sm–Nd approaches (e.g., Maas et al., 1986; Nakai et al., 1990; Christensen et al., 1995; Yang and Zhou, 2001; Zhang et al., 2014). However, Rb, Sr, Sm, and Nd are all lithophile elements (e.g., Faure, 1977) that are incompatible in the majority of sulfides, making the application of these approaches to ore deposits problematic. For example, detailed observations of the sulfides dated by these approaches often identified inclusions of silicate minerals that generated large variations in Rb–Sr or Sm–Nd ratios (Li et al., 2008; Wan et al., 2009). This means that it is often unclear whether the dates acquired by these approaches represent the timing of mineralization or the timing of formation of the silicates that may have formed significantly earlier than the mineralization within a given deposit.

One of the best ways of directly determining the timing of mineralization is Re–Os dating, an approach that uses chalcophile elements that are often enriched in sulfide minerals, thus enabling the direct identification of the timing of mineralization. A significant amount of research has demonstrated the usefulness of molybdenite (MoS_2) for Re–Os dating as this mineral contains both a high concentration of Re (up to hundreds or thousands of parts per million) and very low concentrations of common Os (Luck and Allègre, 1982; Stein et al., 1997; Selby and Creaser, 2001a, 2001b; Wang et al., 2015; Zhang et al., 2016; Gao et al., 2018; Nie et al., 2019). However, molybdenite dating also has some limitations. In some cases, molybdenite Re–Os age and U–Pb zircon ages may be different, with the former often yielding ages that are older than the latter (e.g., Leng et al., 2012; Chen et al., 2015; Zhang et al., 2015; Mao et al., 2017) thus causing confusion over the timing of mineralization. Moreover, molybdenite is not present in all mineral deposits, and other minerals (e.g., pyrite) may be less useful for Re–Os dating.

The Magushan Cu–Mo deposit is a representative example of the skarn mineralization present within the newly discovered Xuancheng ore district of the Middle and Lower Yangtze River Metallogenetic Belt (MLYRMB, Fig. 1). The deposit is a representative example of the skarn mineralization present within the district (Bian, 1995; Liu and Duan, 2015; Hong et al., 2017; Jiang et al., 2017; Qian et al., 2017; Zhou et al., 2017; Fig. 2) and our previous research (Li et al., 2020a) indicates that the mineralization in this area is associated with a porphyritic granodiorite that was emplaced at 134.2 ± 1.2 Ma [mean square weighted deviation (MSWD) = 1.4]. However, this age represents the timing of magmatism in this area and not necessarily the timing of mineralization, although it is very likely that the magmatism and the generation of the skarn in this area are genetically linked as evidenced by paragenetic and spatial relationships (Figs. 3–5). Here, we present new Re–Os dates for molybdenite from the Xuancheng Cu–Mo skarn deposit that suggests that the mineralizing event in this area post-dates the magmatism in this area by around 4 Ma, although both molybdenite Re–Os and zircon U–Pb ages are within uncertainty of each other. This obviously contrasts with the spatial and paragenetic relationships in this area. This, combined with the overlapping uncertainties on the Re–Os and U–Pb ages for the mineralization and magmatism meant

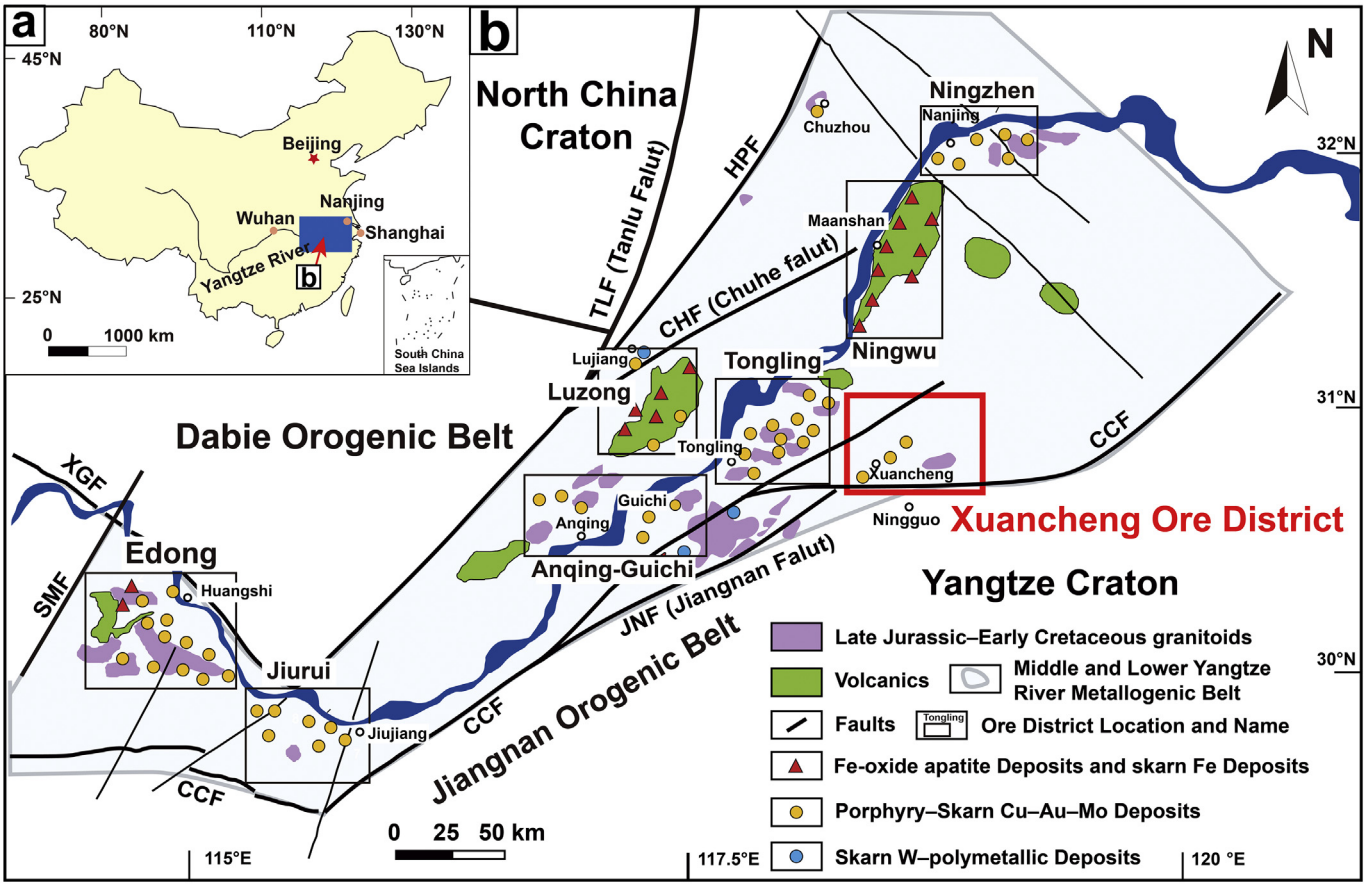

Fig. 1. Geological map of the Middle–Lower Yangtze River Metallogenic Belt showing the location of major ore districts and the study area (modified after Chang et al., 1991; Mao et al., 2011; Zhou et al., 2017).

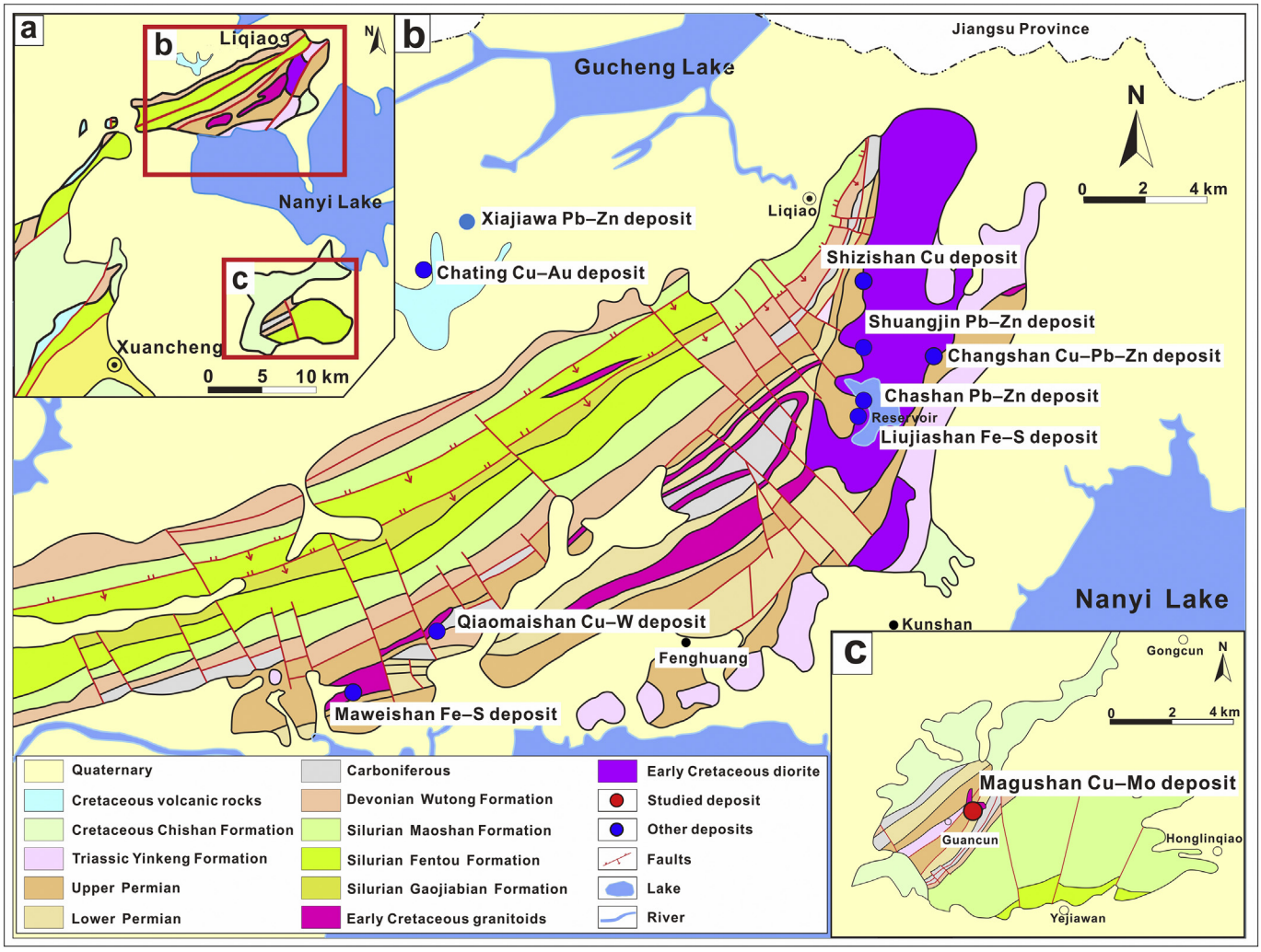

Fig. 2. Sketch map showing the geology of the Xuancheng ore district (modified after Liu and Duan, 2015).

we also undertook titanite and garnet U–Pb dating to try and obtain better constraints in the timing of magmatism and skarn formation, respectively, in this area. Both titanite (Simonetti et al., 2006; Sun et al., 2012; Hu et al., 2017; Song et al., 2019; Xie et al., 2019; Xiao et al., 2020) and garnet (Seman et al., 2017; Fu et al., 2018; Mueller and McNaughton, 2018; Li et al., 2019a) have been dated previously using this approach, indicating this is a viable method for dating these minerals. The new data presented in this study further constrains the timing of magmatism and mineralization associated with the Magushan deposit, furthering our knowledge of the mineralizing processes in this area and providing insights into different methods of determining the relative timing of mineralization and magmatism in similar but more complex systems elsewhere.

2. Geological background

2.1. Regional geology

The MLYRMB is located within the northeastern Yangtze Craton, the southern part of the Qinling–Dabie orogenic belt, and the North China Craton (Chang et al., 1991; Zhai et al., 1996; Yuan et al., 2008; Mao et al., 2011; Zhou et al., 2011, 2015; Pirajno and Zhou, 2015; Fig. 1). It is subdivided into southern, middle and northern subzones (Zhou et al., 2017) and is bounded by the Xiangfan–Guangji Fault (XGF) to the northwest, the Huanglishu–Poliangting Fault (HPF) to the northeast and the Chongyang–Changzhou Fault (CCF) to the south.

The Xuancheng ore district is a newly discovered ore district within the southeast MLYRMB to the east of the Tongling ore district and the south of the Ningwu ore district (Fig. 1). This area represents a newly discovered and relatively unexplored ore district that hosts polymetallic Cu deposits, including the skarn-type Magushan Cu–Mo, Qiaomaishan Cu–W, Shizishan Cu, Changshan Cu–Pb–Zn, and Chashan Pb–Zn deposits as well as the Chating porphyry Cu–Au deposit (Bian, 1995; Hong et al., 2017; Jiang et al., 2017; Qian et al., 2017; Xu et al., 2018; Li et al., 2019c; Fig. 2). The Xuancheng district is dominated by Silurian to Jurassic marine and continental sedimentary rocks (Fig. 2) and hosts generally unexposed and blind mineral deposits that are predominantly covered by Quaternary sediments (Liu and Duan, 2015; Fig. 2). The district also contains Early Cretaceous intrusive units with dominantly granite, granodiorite, and diorite compositions that are closely related to the magmatic–hydrothermal deposits within this area (Liu and Duan, 2015; Li et al., 2019c, 2020a). The Magushan deposit forms the focus of this study, is one of the two largest skarn deposits within this Xuancheng district, and contains some 78,000 t of contained Cu metal at an average grade of 0.89% and 11,000 t of contained Mo at an average grade of 0.13%, with a further 3 t of Au and 300 t of Ag.

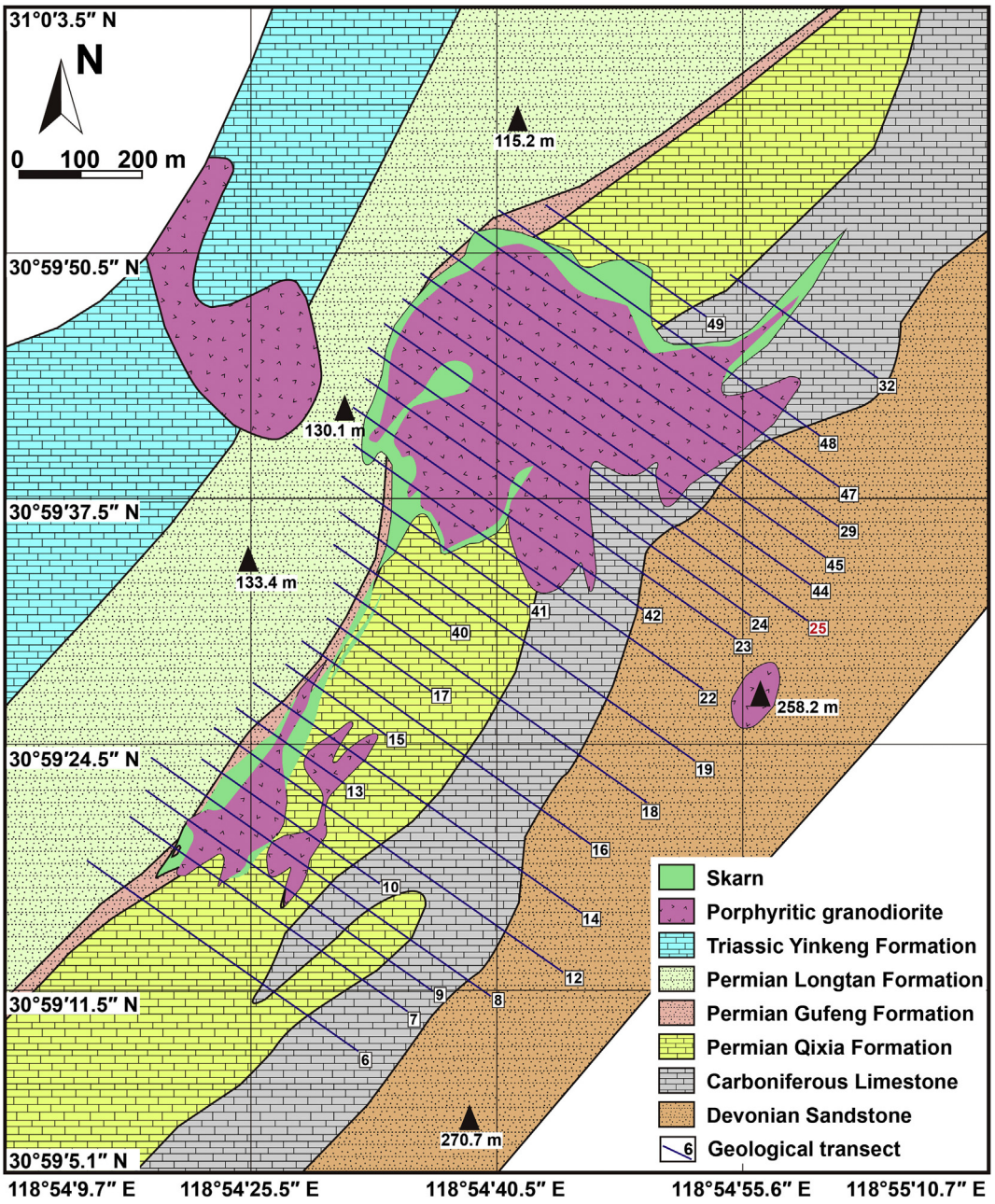

Fig. 3. Geological map showing the area around the Magushan deposit (modified after Bian, 1995; Hong et al., 2017).

2.2. Deposit geology and mineralization

The Magushan Cu–Mo deposit is located east of the city of Xuancheng (Fig. 2a) in an area containing exposed Devonian to Triassic sedimentary units (Fig. 3). The Devonian units in this area are quartz-dominated sandstones with a thickness of about 80–110 m whereas the Carboniferous units are dominated by limestones with a thickness of 150–180 m that have an upper section that also contains some sandstone units. The area also contains Permian limestones of the Qixia Formation with a thickness of 170–300 m and Permian sandstones of the Gufeng and Longtan Formations, with thicknesses of 20 and 300 m, respectively. Argillaceous and hornfels-altered limestones of the Triassic Yinkeng Formation also crop out in this area with a total thickness of >220 m (Bian, 1995; Hong et al., 2017). The majority of the mineralization in this area is hosted by Carboniferous and Permian limestones, with the latter assigned to the Qixia Formation (Bian, 1995; Hong et al., 2017; Fig. 4). The deposit is also genetically associated with a porphyritic granodiorite that is closely spatially related to both orebodies and skarn alteration (Figs. 3 and 4).

The Magushan deposit is located within an inverted anticline (Bian, 1995; Hong et al., 2017; Fig. 4) and the intrusion associated with the deposit was emplaced into the Carboniferous and Permian Qixia Formation limestones that host the majority of the mineralization in this area. This porphyritic granodiorite crops out in various locations within the study area and the petrographic characteristics of the intrusion at these different locations are similar. The intrusion is fresh in areas distal from country rock contacts but has undergone K-feldspar and pyrite alteration near these contacts (Fig. 5a–c). The skarn alteration associated with the deposit is also concentrated within limestones proximal to the porphyritic granodiorite (Figs. 3 and 4). The majority of the orebodies that define the deposit are either layered or lens-shaped and contain chalcopyrite, molybdenite, pyrite, sphalerite, magnetite, and pyrrhotite within a garnet, quartz, and calcite dominated gangue assemblage. Mineralization is

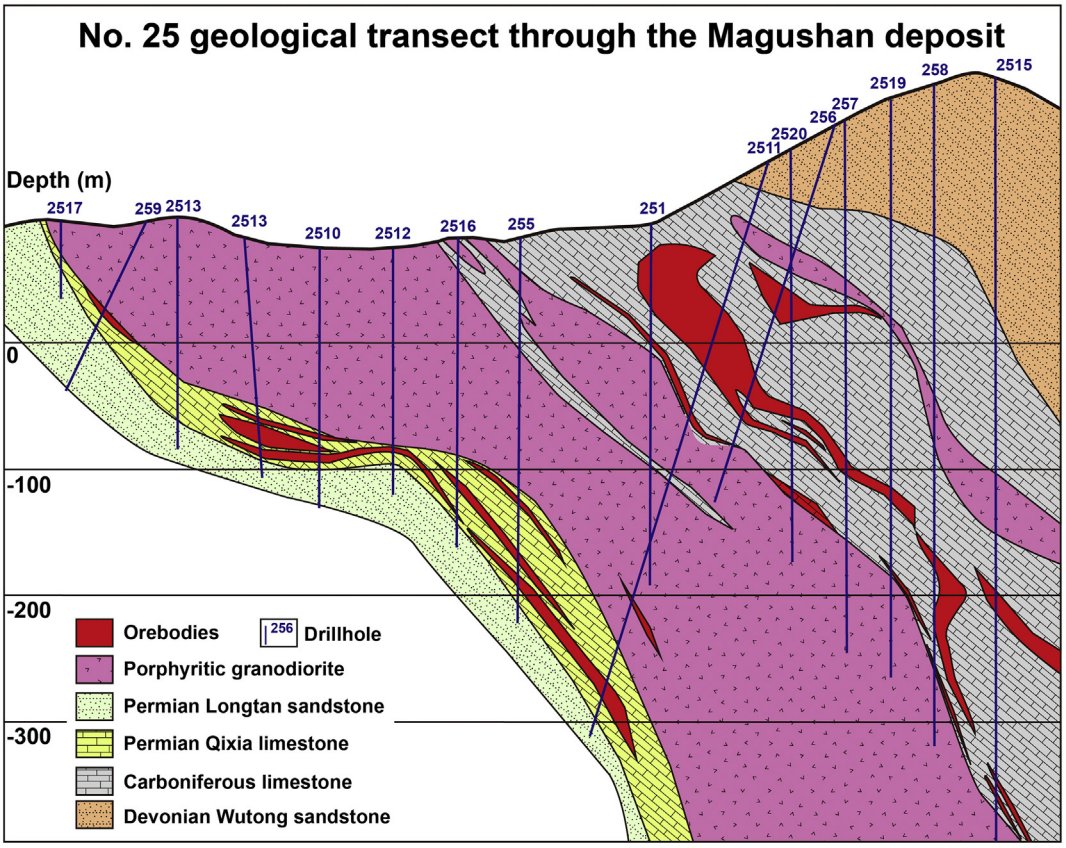

Fig. 4. Cross-section through the Magushan deposit along geological transect No. 25 (modified after Hong et al., 2017).

also present within the porphyritic granodiorite (i.e., endoskarn) and is associated with K-feldspar and pyrite alteration (Fig. 5a–c). However, the majority of mineralization is hosted by Carboniferous and Permian Qixia Formation limestones that have been altered to garnet skarn (Fig. 5d, e) and marble (Fig. 5f), with most of this mineralization hosted by the former (Fig. 5g–i).

3. Samples and analytical methods

The spatial and paragenetic relationships between the intrusions, alteration, and mineralization indicates that the formation of the Magushan deposit is genetically associated with the porphyritic granodiorite (Figs. 3–5). This simple genetic relationship in the Magushan deposit makes this an ideal natural laboratory to test the efficacy of the different geochronometers that can be used on skarn-type mineralizing systems.

3.1. Molybdenite Re–Os dating

Six molybdenite-bearing ore samples associated with garnet skarn in the study area (Fig. 6) were collected from underground developments within the Magushan mine. The samples were crushed to pass ~100–150 meshes before molybdenite was separated using standard heavy liquid separation techniques. High-purity (>99%) molybdenite separates were then obtained by handpicking under a binocular microscope. Re–Os isotopic analysis was undertaken at the Re–Os Laboratory of the National Research Center of Geoanalysis, Chinese Academy of Geological Sciences (CAGS), Beijing, China. This analysis used the chemical separation approaches outlined in Shirey and Walker (1995), Markey et al. (1998), Mao et al. (1999, 2006), Stein et al. (2001), and Du et al. (2004).

Prior to analysis enriched ^{190}Os and ^{185}Re spikes were obtained from Oak Ridge National Laboratory in the USA. Weighed unknowns (~ 0.01 g) were loaded into Carius tube using a thin neck funnel before mixed ^{190}Os and ^{185}Re spike solutions combined with 2 mL HCl and 4 mL HNO_4 were added while the base of the tubes was frozen at temperatures between −50 °C and − 80 °C in an ethanol–liquid nitrogen slush. The tops of the Carius tubes were then sealed using an oxygen-propane torch and the tubes were then placed in stainless steel jackets before being heated for 24 h at 230 °C. The tubes were then cooled, with the base of the tubes being frozen while the necks of the tubes were broken. This allowed the removal of Os from the Carius tube by direct distillation for a period of 50 min, with the removed Os trapped in 3 mL of water that was subsequently used for the determination of Os isotopic ratios. This analysis used multicollector–inductively coupled plasma–mass spectroscopy (MC–ICP–MS) employing a Neptune Plus instrument at the Re–Os Laboratory of the National Research Center of Geoanalysis, CAGS, Beijing, China. The residual Re-bearing solution was saved in a 150 mL Teflon beaker for subsequent Re separation.

Rhenium isotopic analysis used the residual Re-bearing solution that was heated to near-dryness before the addition of 5 mL of 30% NaOH to the residue followed by Re extraction using 5 mL of acetone in a 50 mL centrifuge tube. The Re-bearing acetone phase was then transferred to 150 mL Teflon beakers that contained 1 mL of water. This solution was then evaporated to dryness before the addition of 2% HNO_3 for the ICP–MS determination of Re isotopic ratios using an X-series instrument at Re–Os Laboratory of the National Research Center of Geoanalysis, CAGS, Beijing, China.

3.2. Titanite U–Pb dating

Titanite was obtained from fresh porphyritic granodiorite samples distal from the skarn alteration associated with the contact between the intrusion and the surrounding limestones (Fig. 7). Polished thin sections were made from these samples and were used to identify titanite

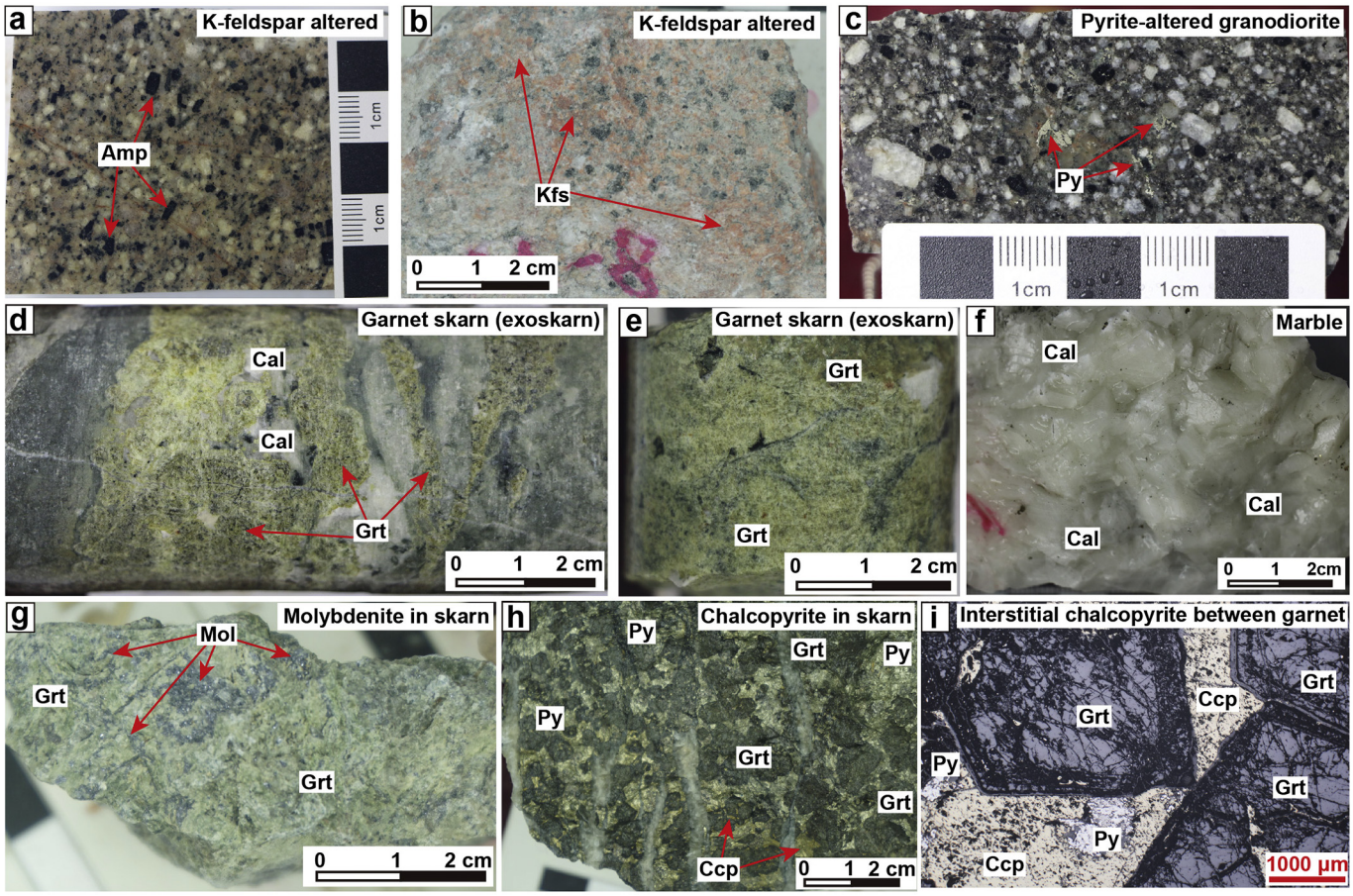

Fig. 5. Photographs of hand specimens from the Magushan deposit showing representative examples of alteration and mineralization within the study area. (a, b) K-feldspar-bearing porphyritic granodiorite. (c) Pyrite alteration within the porphyritic granodiorite. (d, e) Andradite garnet exoskarn associated with the Magushan deposit. (f) Marble-altered limestone. (g, h) Molybdenite, chalcopyrite, and pyrite mineralization within garnet skarn. (i) Photomicrograph taken under reflected light showing a typical example of the mineralized garnet skarn. Abbreviations are as follows: Amp = amphibole, Kfs = K-feldspar, Py = pyrite, Cal = calcite, Grt = garnet, Mol = molybdenite, Ccp = chalcopyrite.

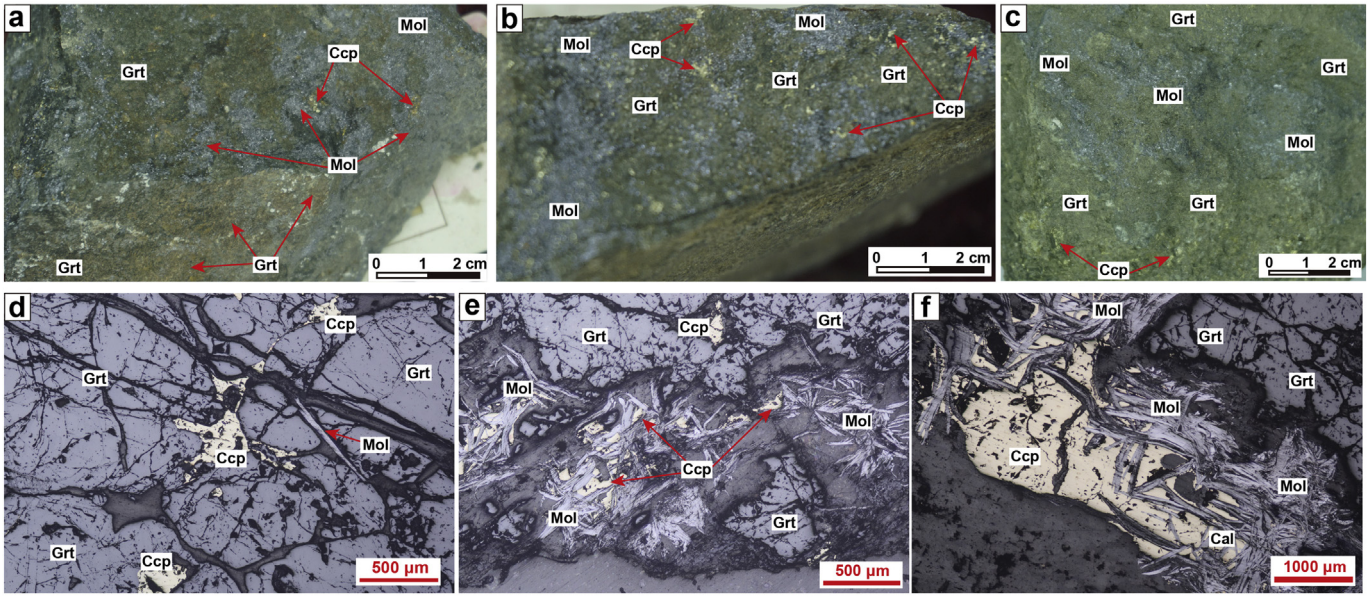

Fig. 6. Photographs (a–c) and photomicrographs (d–f) showing representative examples of the molybdenite ore from the Magushan deposit. (a–c) Hand specimens of molybdenite mineralization hosted by garnet skarn. (d–f) Photomicrographs taken under reflected light showing molybdenite mineralization hosted by garnet skarn. Abbreviations are as in Fig. 5.

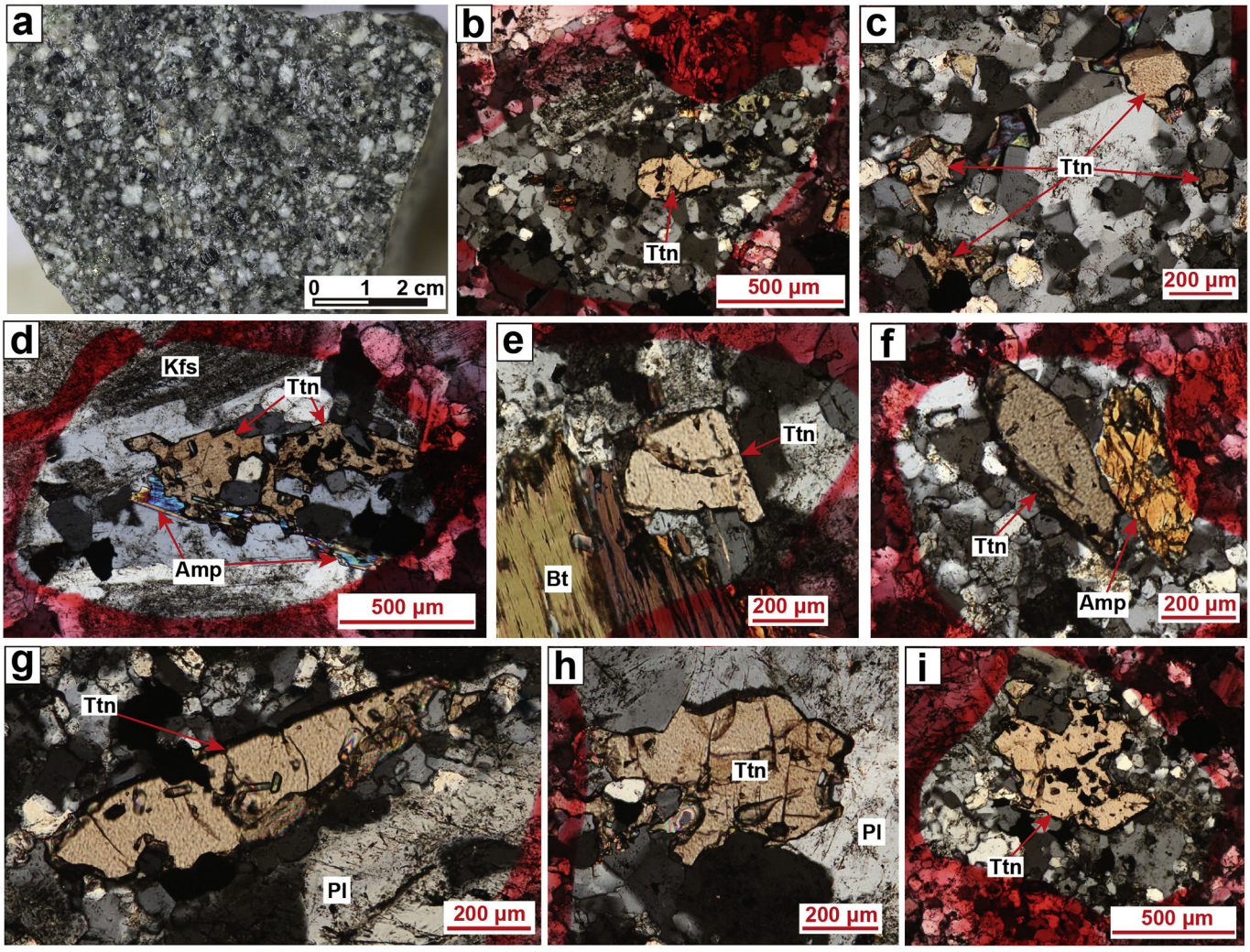

Fig. 7. Images showing representative examples of the fresh porphyritic granodiorite and the location and characteristics of the titanite within this intrusion. (a) Hand specimen showing a representative example of the porphyritic granodiorite. (b–i) Photomicrographs were taken under cross-polarized light showing some of the titanite analyzed during this study. Abbreviations are as follows: Ttn = titanite, Bt = biotite, Pl = plagioclase.

using standard optical microscopy. Titanite is a common accessory mineral within the intrusion associated with the Magushan deposit and is generally 100–800 μm long (Fig. 7b–i). A total of 30 titanite crystals from two polished thin sections were dated during this study.

The in-situ U–Pb dating of titanite was undertaken using laser ablation–ICP–MS (LA–ICP–MS) at the Ore Deposit and Exploration Centre (ODEC), School of Resources and Environmental Engineering, Hefei University of Technology, Hefei, China. Details of the LA–ICP–MS specifications and operating conditions used during this study are given in Appendix 1. These analyses used a PhotonMachines Analyte HE LA system equipped with a 193 nm ArF Excimer laser that was coupled to an Agilent 7900 quadrupole ICP–MS instrument. Ablation was undertaken in an ultrahigh purity He atmosphere (0.9 L/min) mixed with Ar (0.9 L/min) using a 40 μm diameter laser beam. Three standards were used during this analysis with an OLT-1 titanite standard (Kennedy et al., 2010) used for calibration, mass discrimination, and isotope fractionation. A BLR-1 titanite (1047.1 ± 0.4 Ma; Aleinikoff et al., 2007; Mazdab, 2009) standard was also analyzed as an age monitor during routine analysis to determine the precision and accuracy of the analysis of unknowns and a GSE-1G silicate glass standard was used for the external standardization of trace element compositions. Each analysis incorporated a background acquisition time of approximately 20 s (gas blank) followed by 40 s of data acquisition time during the ablation of the sample. Off-line selection and integration of background and analytical signals, time drift corrections, and the quantitative calibration of titanite trace-element concentrations and U–Pb ages were all undertaken using the ICPMSDataCal software package (Liu et al., 2010b). Measured uncorrected titanite data were plotted on a Tera–Wasserburg diagram (Tera and Wasserburg, 1972) defining a line that yields a lower intercept age that approximates the timing of formation of the sample.

3.3. Garnet U–Pb dating

The garnet samples used for U–Pb dating during this study were taken from underground developments within the Magushan mine and drillcore. These samples were taken from both endoskarn and exoskarn settings but the exoskarn andradite garnet present in the latter contains higher concentrations of U (Li et al., 2020b in review), making it more suitable for use during U–Pb dating. The exoskarn andradite garnet is also genetically associated with the mineralization in this area, indicating the timing of both garnet formation and mineralization may be recorded by the age of these minerals (Fig. 8). Andradite garnet from a total of four polished thin sections were dated during this

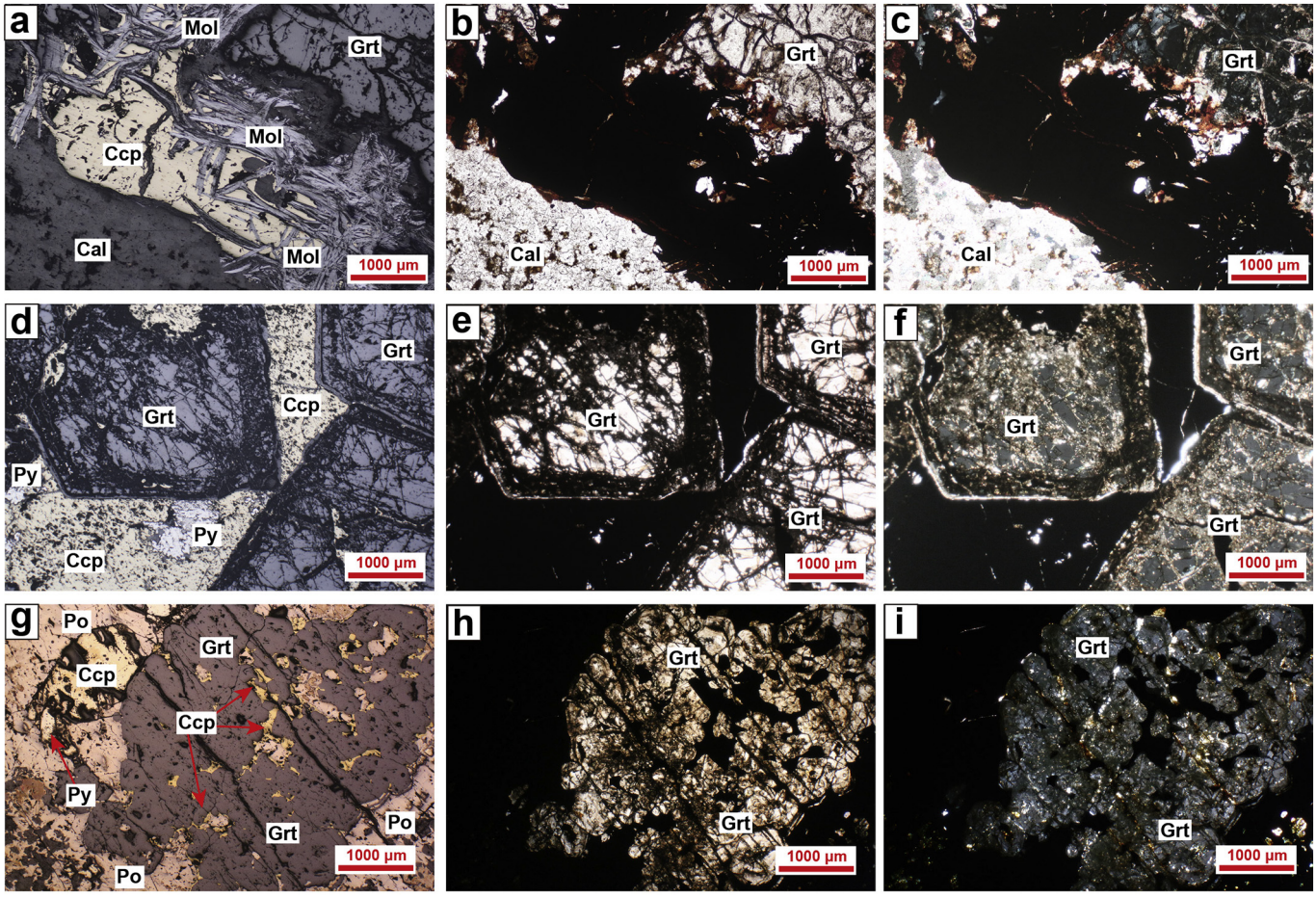

Fig. 8. Photomicrographs showing representative examples of mineralized garnet skarn within the Magushan deposit; the same sample is shown in each row. (a, d, g) Photomicrographs of mineralized garnet skarn taken under reflected light. (b, e, h) Photomicrographs of mineralized garnet skarn taken under plane-polarized light. (c, f, i) Photomicrographs of mineralized garnet skarn taken under cross-polarized light. Abbreviations are as in Fig. 5 with Po = pyrrhotite.

study using LA–ICP–MS at the Ore Deposit and Exploration Centre (ODEC), School of Resources and Environmental Engineering, Hefei University of Technology, Hefei, China. These analyses used the same instrument and parameters used for titanite dating with a 40 μm diameter laser beam (Appendix 1). A ZK803–97 garnet standard (Zhang et al., 2019) was used for calibration, mass discrimination, and isotope fractionation, with an OH-1 garnet standard (Seman et al., 2017; Zhang et al., 2019) analyzed as an age monitor during routine analysis to monitor analytical accuracy and a precision. A GSE-1G silicate glass standard was also used for the external standardization of trace element compositions.

4. Results

4.1. Molybdenite Re–Os ages

The results of the Re–Os isotopic analysis of the six molybdenite samples from the Magushan deposit as well as blank and standard data are given in Table 1 with Re–Os isochron and weighted mean molybdenite model ages shown in Fig. 9. The molybdenite model ages were calculated using $t = [\ln(1 + {}^{187}Os/{}^{187}Re)]/\lambda$, where λ is the ^{187}Re decay constant of 1.666×10^{-11} year^{-1} (Smoliar et al., 1996). We used an initial $^{187}Re/^{188}Os$–$^{187}Os/^{188}Os$ ratio isoline to remove the non-radiogenic

Table 1
Molybdenite Re–Os isotopic data for the Magushan deposit.

Sample	Weight (g)	Re		^{187}Re		Common Os		^{187}Os		Model age	
		(ppb)	±1σ	(ppb)	±1σ	(ppb)	±1σ%	(ppb)	±1σ	Age (Ma)	Uncertainty
MGS-Mo-1	0.01022	89,736	935	56,401	588	0.00192	0.60350	131.4	1.0	139.1	1.8
MGS-Mo-2	0.01081	88,682	867	55,738	545	0.00310	0.06846	128.1	0.8	137.1	1.6
MGS-Mo-3	0.01035	58,563	541	36,808	340	0.18917	0.20169	84.8	0.6	137.1	1.6
MGS-Mo-4	0.01042	88,950	1038	55,907	652	0.69151	0.13994	130.1	1.0	138.9	1.9
MGS-Mo-5	0.01109	21,637	166	13,600	105	0.00174	0.04001	31.9	0.3	138.0	1.8
MGS-Mo-6	0.01053	54,929	413	34,524	260	0.22464	0.06380	79.4	0.5	136.8	1.4
Blank sample	–	0.00400	0.00064	–	–	0.00000	0.00172	0.00009	0.00043	–	–
Standard	Weight (g)	Re (ppm)	±1σ					^{187}Os (ppb)	±1σ	Age (Ma)	uncertainty
GBW04435(HLP)	0.00641	274.8	2.7	–	–	–	–	640.5	4	222.2	3.4
Reference values	–	283.8	6.2	–	–	–	–	659	14.4	221.4	5.6

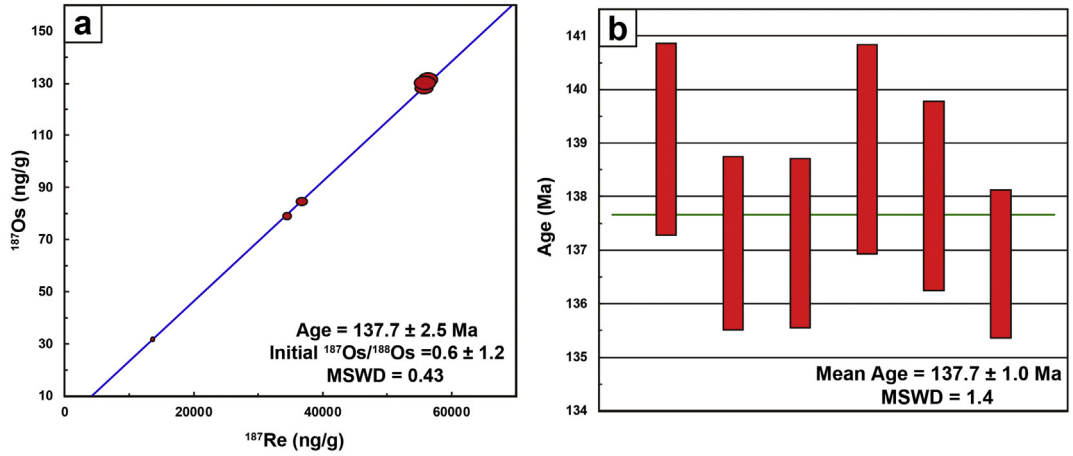

Fig. 9. Re–Os isochron age (a) and weighted mean model age (b) diagrams showing variations in ages of molybdenite within the Magushan deposit.

^{187}Os from each sample (Li et al., 2012), yielding model ages. Isochron and weighted average ages were also calculated for each sample. The Re content of these samples is 21.6 to 89.7 ppm (average of 60.7 ppm). The six molybdenite samples analyzed during this study yield model ages between 139.1 Ma, 138.9 Ma, 138.0 Ma, 137.1 Ma, 137.1 Ma, and 136.8 Ma and define a well-constrained ^{187}Re–^{187}Os isochron age of 137.7 ± 2.5 Ma (2σ, n = 6, MSWD = 0.43; Fig. 9a) and a weighted mean model age of 137.7 ± 1.0 Ma (2σ, MSWD = 1.4; Fig. 9b).

4.2. Titanite and garnet U–Pb ages

The titanite U–Pb isotopic data obtained during this study are given in Table 2 and are shown in Fig. 10a. The U–Pb isotope data for these titanite samples are plotted on a Tera–Wasserburg diagram and define a regression line that yields a well-defined lower-intercept age of 136.3 ± 2.5 Ma (2σ, n = 30, MSWD = 3.2; Fig. 10a). The andradite garnet U–Pb isotopic data are given in Table 3, and plotting these data on a Tera–Wasserburg diagram (Fig. 10b) yields a well-defined lower-intercept age of 135.9 ± 2.7 Ma (2σ, n = 30, MSWD = 2.5). The results of the analysis of the standards undertaken during this study are given in Table 4. Analysis of the OLT-1 titanite standard (1016.8 ± 3.8 Ma; Kennedy et al., 2010) during titanite U–Pb dating yielded a well-defined lower-intercept age of 1021 ± 13 Ma (2σ, n = 8, MSWD = 2.9; Fig. 10c) and the age monitor BLR-1 titanite standard (1047.1 ± 0.4 Ma; Aleinikoff et al., 2007; Mazdab, 2009) yielded a well-defined lower-intercept age of 1045 ± 20 Ma (2σ, n = 8, MSWD = 0.49; Fig. 10d). The andradite garnet dating included analysis of the ZK803–97 garnet standard (139.1 ± 1.0 Ma; Zhang et al., 2019), yielding a well-defined lower-intercept age of 137.8 ± 3.1 Ma (2σ, n = 7,

Table 2
Titanite U–Pb isotopic data for the Magushan deposit.

Spots	^{207}Pb/^{235}U		^{206}Pb/^{238}U		^{207}Pb/^{206}Pb		^{206}Pb/^{238}U		Pb	Th	U
	Ratio	±1σ	Ratio	±1σ	Ratio	±1σ	Age (Ma)	±1σ	ppm	ppm	ppm
MGS-Ttn-1	0.25621	0.01066	0.02332	0.00049	0.08187	0.00352	148.6	3.1	0.00	510.0	181.6
MGS-Ttn-2	0.25079	0.01115	0.02173	0.00030	0.08317	0.00309	138.6	1.9	1.99	1106.2	519.7
MGS-Ttn-3	0.30524	0.01380	0.02223	0.00039	0.10178	0.00470	141.7	2.5	1.47	247.7	200.4
MGS-Ttn-4	0.18247	0.00896	0.02155	0.00038	0.06234	0.00307	137.4	2.4	3.55	425.9	232.4
MGS-Ttn-5	0.23408	0.00857	0.02223	0.00038	0.07670	0.00274	141.7	2.4	0.00	386.7	272.8
MGS-Ttn-6	0.94707	0.04118	0.03123	0.00090	0.24035	0.01383	198.3	5.6	3.70	359.0	55.8
MGS-Ttn-7	0.16156	0.00490	0.02219	0.00034	0.05332	0.00162	141.5	2.1	2.99	1247.9	627.3
MGS-Ttn-8	0.55216	0.03284	0.02568	0.00058	0.15393	0.00840	163.4	3.6	3.95	217.6	152.7
MGS-Ttn-9	0.20197	0.00861	0.02193	0.00034	0.06796	0.00305	139.8	2.2	0.00	462.0	222.4
MGS-Ttn-10	0.96927	0.03641	0.02941	0.00086	0.27522	0.01542	186.9	5.4	4.52	336.5	56.8
MGS-Ttn-11	0.77734	0.03276	0.02818	0.00073	0.22483	0.01245	179.1	4.6	3.12	394.8	82.5
MGS-Ttn-12	0.21372	0.00758	0.02146	0.00035	0.07286	0.00255	136.9	2.2	0.00	715.6	364.4
MGS-Ttn-13	0.34642	0.01672	0.02422	0.00058	0.11111	0.00620	154.2	3.7	0.55	303.2	124.6
MGS-Ttn-14	1.17623	0.05505	0.03246	0.00085	0.25464	0.00941	205.9	5.3	8.73	262.0	142.4
MGS-Ttn-15	0.42787	0.01694	0.02361	0.00052	0.13936	0.00605	150.4	3.3	0.57	455.3	136.7
MGS-Ttn-16	0.38387	0.01325	0.02377	0.00053	0.12150	0.00432	151.4	3.3	5.43	496.5	150.3
MGS-Ttn-17	0.25861	0.01304	0.02298	0.00055	0.08720	0.00574	146.4	3.5	3.60	341.3	105.6
MGS-Ttn-18	0.20257	0.00970	0.02216	0.00036	0.06664	0.00314	141.3	2.3	0.37	313.3	187.9
MGS-Ttn-19	0.19653	0.00635	0.02129	0.00033	0.06734	0.00218	135.8	2.1	1.09	459.0	318.7
MGS-Ttn-20	0.77993	0.03147	0.02788	0.00077	0.22494	0.01197	177.3	4.9	4.37	442.0	63.9
MGS-Ttn-21	0.93465	0.03887	0.02860	0.00081	0.27047	0.01613	181.8	5.1	3.50	342.2	50.9
MGS-Ttn-22	0.89594	0.03464	0.03127	0.00087	0.22656	0.01017	198.5	5.4	2.94	353.6	56.7
MGS-Ttn-23	0.91130	0.03281	0.02853	0.00072	0.24914	0.01054	181.3	4.5	0.00	413.5	67.7
MGS-Ttn-24	0.35923	0.01597	0.02350	0.00045	0.11430	0.00514	149.7	2.9	1.02	253.5	122.9
MGS-Ttn-25	0.30978	0.01176	0.02396	0.00044	0.09602	0.00370	152.6	2.8	3.69	485.4	199.1
MGS-Ttn-26	0.20433	0.01067	0.02230	0.00060	0.07283	0.00545	142.1	3.8	2.48	116.8	64.8
MGS-Ttn-27	0.24712	0.01634	0.02327	0.00053	0.08104	0.00599	148.3	3.4	0.00	243.4	106.7
MGS-Ttn-28	0.28350	0.00935	0.02380	0.00039	0.08868	0.00305	151.6	2.5	2.02	315.3	213.7
MGS-Ttn-29	0.82723	0.03033	0.02796	0.00075	0.23419	0.01112	177.8	4.7	1.38	628.7	83.9
MGS-Ttn-30	0.42449	0.01880	0.02406	0.00056	0.13985	0.00857	153.3	3.5	2.94	423.5	95.2

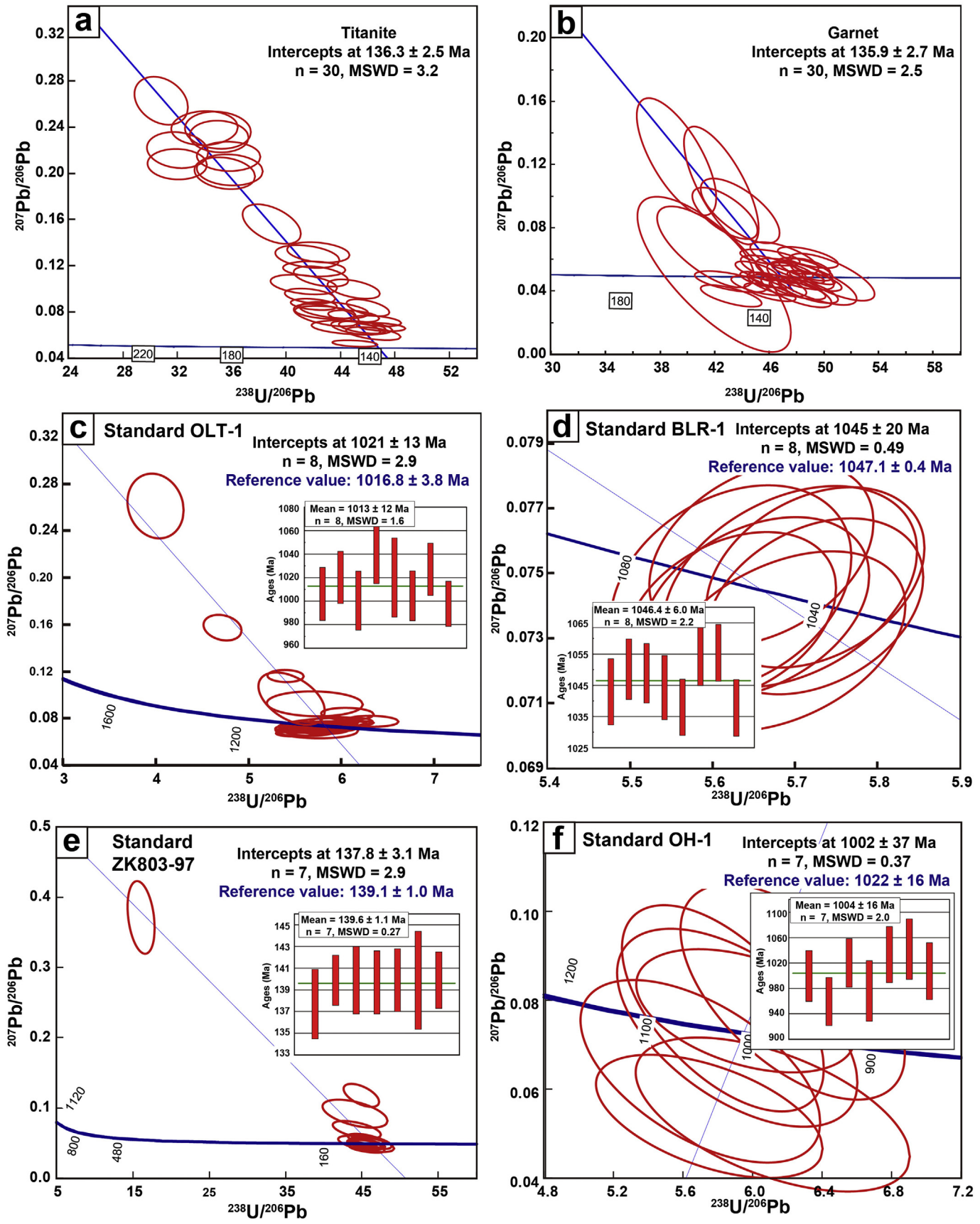

Fig. 10. Tera–Wasserburg diagrams showing U–Pb ages for the titanite (a) and andradite garnet (b) samples from the Magushan deposit. (c–f) Tera–Wasserburg and weighted average diagrams showing the results of the analysis of standards undertaken during this study.

Table 3
Andradite garnet U–Pb isotopic data for the Magushan deposit.

Spots	$^{207}Pb/^{235}U$		$^{206}Pb/^{238}U$		$^{207}Pb/^{206}Pb$		$^{206}Pb/^{238}U$		Pb	Th	U
	Ratio	±1σ	Ratio	±1σ	Ratio	±1σ	Age (Ma)	±1σ	ppm	ppm	ppm
MGS-GRT-1	0.17824	0.02436	0.02123	0.00074	0.06918	0.01639	135.4	4.7	0.24	0.007	5.6
MGS-GRT-2	0.12612	0.02993	0.02036	0.00090	0.05104	0.01743	129.9	5.7	1.32	0.013	4.3
MGS-GRT-3	0.14573	0.02310	0.02089	0.00083	0.05747	0.01446	133.3	5.2	0.17	0.019	5.0
MGS-GRT-4	0.11350	0.01719	0.02046	0.00061	0.04570	0.00820	130.6	3.8	0.82	0.078	9.6
MGS-GRT-5	0.15596	0.01232	0.02041	0.00041	0.06295	0.00528	130.3	2.6	2.15	0.021	24.0
MGS-GRT-6	0.12987	0.01484	0.02028	0.00054	0.05277	0.00709	129.4	3.4	1.27	0.002	10.6
MGS-GRT-7	0.13288	0.03074	0.01978	0.00081	0.05536	0.03005	126.2	5.1	2.20	0.032	4.5
MGS-GRT-8	0.11707	0.01425	0.02081	0.00059	0.04636	0.00685	132.7	3.7	1.36	0.008	9.6
MGS-GRT-9	0.13836	0.01039	0.02169	0.00045	0.05256	0.00437	138.3	2.9	0.84	0.107	29.2
MGS-GRT-10	0.11733	0.01392	0.02171	0.00059	0.04452	0.00579	138.5	3.7	1.23	0.010	13.5
MGS-GRT-11	0.22683	0.06629	0.02419	0.00137	0.07725	0.03551	154.1	8.6	0.76	0.003	2.3
MGS-GRT-12	0.18368	0.01424	0.02172	0.00068	0.06968	0.00768	138.5	4.3	0.54	0.206	9.6
MGS-GRT-13	0.16605	0.11801	0.02383	0.00210	0.05741	0.03795	151.8	13.2	1.38	0.019	1.4
MGS-GRT-14	0.13104	0.01795	0.02148	0.00066	0.05025	0.00855	137.0	4.2	2.23	0.421	8.6
MGS-GRT-15	0.43949	0.10226	0.02550	0.00125	0.14195	0.02381	162.3	7.9	2.31	0.011	3.2
MGS-GRT-16	0.28483	0.05173	0.02280	0.00099	0.10293	0.02121	145.3	6.2	1.80	0.009	3.6
MGS-GRT-17	0.13210	0.01505	0.02209	0.00067	0.04925	0.01073	140.9	4.2	0.96	0.626	8.8
MGS-GRT-18	0.11493	0.02242	0.02085	0.00074	0.04541	0.01123	133.0	4.7	1.54	0.061	7.1
MGS-GRT-19	0.14354	0.01200	0.02204	0.00049	0.05364	0.00508	140.5	3.1	1.76	0.210	30.0
MGS-GRT-20	0.34613	0.09117	0.02353	0.00100	0.12116	0.02234	149.9	6.3	2.05	0.021	4.6
MGS-GRT-21	0.14628	0.01827	0.02316	0.00094	0.05204	0.01946	147.6	5.9	0.32	0.025	5.4
MGS-GRT-22	0.16239	0.01441	0.02219	0.00051	0.06029	0.00632	141.5	3.2	0.29	0.711	43.6
MGS-GRT-23	0.11775	0.01759	0.02315	0.00079	0.04191	0.01003	147.5	5.0	1.96	0.038	5.8
MGS-GRT-24	0.28776	0.04240	0.02339	0.00086	0.10135	0.01534	149.0	5.4	1.23	0.065	7.9
MGS-GRT-25	0.15281	0.01178	0.02096	0.00044	0.06007	0.00569	133.7	2.8	1.36	1.274	23.6
MGS-GRT-26	0.13774	0.00870	0.02050	0.00035	0.05534	0.00395	130.8	2.2	1.08	1.169	47.3
MGS-GRT-27	0.17278	0.01632	0.02048	0.00061	0.06951	0.00845	130.7	3.8	0.56	0.091	8.1
MGS-GRT-28	0.16002	0.02172	0.02159	0.00074	0.06106	0.01228	137.7	4.7	1.53	0.043	6.5
MGS-GRT-29	0.13283	0.00806	0.02016	0.00032	0.05428	0.00338	128.7	2.0	0.57	0.029	67.7
MGS-GRT-30	0.15240	0.01674	0.02055	0.00055	0.06109	0.00813	131.1	3.5	0.64	0.048	14.1

MSWD = 2.9; Fig. 10e) and an age monitor OH-1 garnet standard that is compositionally similar to the Willsboro garnet standard and has a similar U–Pb age (1022 ± 16 Ma; Seman et al., 2017). Analysis of the latter yielded a well-defined lower-intercept age of 1002 ± 37 Ma (2σ, $n = 7$, MSWD = 0.37; Fig. 10f). The weighted average ages obtained during the analysis of the secondary standards used during this study are also given in Fig. 10c–f. These data are consistent with the lower-intercept ages obtained from the Tera–Wasserburg diagrams shown within the same figure and are within uncertainty of the reported reference ages for these standards. These data also have centralized distributions rather than being overdispersed (e.g., Spencer et al., 2016; Fig. 10c–f). All of this indicates that the ages obtained during the analysis of unknowns are both accurate and precise.

5. Discussion

5.1. Molybdenite Re–Os age

Molybdenite provides robust Re–Os ages because it contains abundant Re and negligible initial or common Os (Markey et al., 1998; Selby and Creaser, 2001a, 2001b, 2004; Stein et al., 2001), and the closure temperature of the Re–Os isotope system for molybdenite is estimated to be around 500 °C (Gao et al., 2017; Li et al., 2019b). This means that molybdenite is somewhat less sensitive to later hydrothermal, metamorphic, and/or tectonic events than other dateable ore minerals, indicating that molybdenite Re–Os dating often (but not always) yields precise ages that reflect the timing of ore deposit formation (e.g. Stein et al., 1997, 2001; Selby and Creaser, 2001a, 2001b, 2004; Bingen and Stein, 2003; Hu et al., 2012).

Our previous research (Li et al., 2020a) determined a zircon U–Pb age of 134.2 ± 1.2 Ma (MSWD = 0.43) for the mineralization-related porphyritic granodiorite in the study area. The new molybdenite Re–Os dating during this study yielded an isochron age of 137.7 ± 2.5 Ma (2σ, $n = 6$, MSWD = 0.43; Fig. 9a) which is within uncertainty of the zircon U–Pb age of the intrusion. The consistent nature of the isochron (137.7 ± 2.5 Ma; Fig. 9a) and weighted mean (137.7 ± 1.0 Ma; Fig. 9b) model Re–Os ages indicates they are reliable (Stein et al., 1997; Selby and Creaser, 2001a). However, there is a relatively large gap between the molybdenite Re–Os and zircon U–Pb ages that outline the timing of mineralization and intrusion, respectively. This is despite the presence of spatial relationships between hydrothermal alteration and the intrusion (Fig. 4) and paragenetic relationships between mineralization, alteration, and the intrusion (Fig. 5), both of which provide evidence of a genetic relationship between mineralization and the emplacement of the porphyritic granodiorite in the study area. This suggests that other approaches to constraining the relative timing of events and geochronological relationships are needed in this area. This would also be important in areas containing complexly zoned plutons with multiple intrusive phases that are not clearly linked with mineralization or in areas with distal skarn mineralization that has no clear spatial relationship to a pluton. Both of these more complex situations mean that any overlapping uncertainties relating to Re–Os and U–Pb ages would make it impossible to determine if a genetic relationship exists between mineralization and intrusive events and/or determine whether an area records a single or multiple phase of magmato-hydrothermal activity. Some research has also suggested that the Re–Os dating of molybdenite yields ages that are often older than the results of U–Pb dating (Chen et al., 2015; Zhang et al., 2015; Gao et al., 2017; Mao et al., 2017), adding further uncertainty to the determination of genetic relationships between mineralization and intrusive events. All of this suggests that further geochronological data are needed to identify genetic relationships in situations more complex than those present within the study area. Here, we present alternative approaches to dating the timing of skarn formation and intrusion that although confirming the relationships within the study area also provide a template for approaches to determine timing relationships within more complex systems.

Table 4
Results of the analysis of the titanite and garnet standards used during the U–Pb dating undertaken in this study.

Mineral	Standard and spot number	$^{207}Pb/^{235}U$		$^{206}Pb/^{238}U$		$^{207}Pb/^{206}Pb$		$^{207}Pb/^{235}U$		$^{206}Pb/^{238}U$	
		Ratio	±1σ	Ratio	±1σ	Ratio	±1σ	Age (Ma)	±1σ	Age (Ma)	±1σ
Titanite	BLR-1std-1	1.80600	0.02999	0.17562	0.00194	0.07465	0.00123	1047.6	10.9	1043.0	10.6
	BLR-1std-2	1.80380	0.02717	0.17694	0.00177	0.07387	0.00109	1046.8	9.9	1050.2	9.7
	BLR-1std-3	1.84193	0.02767	0.17669	0.00173	0.07567	0.00116	1060.6	9.9	1048.9	9.5
	BLR-1std-4	1.76787	0.02631	0.17587	0.00187	0.07284	0.00098	1033.7	9.7	1044.3	10.3
	BLR-1std-5	1.78227	0.02636	0.17470	0.00164	0.07411	0.00107	1039.0	9.6	1038.0	9.0
	BLR-1std-6	1.82753	0.03180	0.17786	0.00189	0.07441	0.00111	1055.4	11.4	1055.3	10.3
	BLR-1std-7	1.80645	0.02590	0.17789	0.00166	0.07367	0.00103	1047.8	9.4	1055.4	9.1
	BLR-1std-8	1.80335	0.02703	0.17467	0.00165	0.07484	0.00109	1046.7	9.8	1037.8	9.1
	GSE-1G-1	24.84925	1.15712	0.27452	0.00872	0.65576	0.02996	3302.3	45.5	1563.7	44.1
	GSE-1G-2	25.47003	0.26902	0.27685	0.00256	0.66605	0.00597	3326.4	10.6	1575.5	12.9
	GSE-1G-3	24.95983	0.25856	0.26976	0.00239	0.67085	0.00597	3306.6	10.4	1539.6	12.2
	GSE-1G-4	25.56633	0.30209	0.27276	0.00275	0.68001	0.00765	3330.1	11.8	1554.8	13.9
	OLT-1-1	1.72688	0.03835	0.16894	0.00409	0.07377	0.00125	1018.6	14.3	1006.3	22.6
	OLT-1-2	1.75218	0.03610	0.17149	0.00403	0.07371	0.00128	1028.0	13.3	1020.3	22.2
	OLT-1-3	1.71370	0.03620	0.16791	0.00453	0.07427	0.00147	1013.7	13.6	1000.6	25.0
	OLT-1-4	1.73175	0.04889	0.17537	0.00484	0.07114	0.00131	1020.4	18.2	1041.6	26.6
	OLT-1-5	1.78247	0.06244	0.17149	0.00610	0.07502	0.00172	1039.1	22.8	1020.3	33.6
	OLT-1-6	1.73714	0.03697	0.16866	0.00383	0.07441	0.00119	1022.4	13.7	1004.7	21.2
	OLT-1-7	1.75033	0.03815	0.17274	0.00406	0.07315	0.00102	1027.3	14.1	1027.2	22.3
	OLT-1-8	1.72264	0.03166	0.16742	0.00346	0.07437	0.00106	1017.0	11.8	997.9	19.1
Garnet	GSE-1G-1	27.99784	1.48401	0.27123	0.00413	0.85047	0.04315	3419.0	52.0	1547.0	20.9
	GSE-1G-2	20.52502	0.92206	0.27090	0.00416	0.62354	0.02631	3116.4	43.5	1545.4	21.1
	GSE-1G-3	18.79892	0.91795	0.26935	0.00447	0.57500	0.02793	3031.6	47.1	1537.5	22.7
	GSE-1G-4	27.12701	1.02189	0.27324	0.00350	0.81810	0.03127	3388.1	37.0	1557.2	17.8
	OH-1-1	1.79484	0.17792	0.16778	0.00724	0.08813	0.02327	1043.6	64.6	999.8	40.0
	OH-1-2	1.80996	0.27047	0.16051	0.00680	0.09290	0.01347	1049.1	97.7	959.6	37.8
	OH-1-3	1.84827	0.27531	0.17151	0.00698	0.08878	0.01396	1062.8	98.1	1020.4	38.4
	OH-1-4	1.22352	0.20219	0.16349	0.00860	0.06165	0.01054	811.4	92.3	976.2	47.7
	OH-1-5	1.29214	0.17446	0.17388	0.00804	0.06120	0.00850	842.2	77.3	1033.4	44.2
	OH-1-6	1.54838	0.25329	0.17544	0.00869	0.07266	0.01245	949.8	100.9	1042.0	47.6
	OH-1-7	1.72162	0.26663	0.16912	0.00809	0.08388	0.01632	1016.6	99.5	1007.3	44.6
	zk803–97A-1	0.36211	0.02586	0.02226	0.00047	0.13400	0.01023	145.7	12.9	137.7	3.2
	zk803–97A-2	0.15425	0.01466	0.02159	0.00050	0.05887	0.00622	140.0	8.5	139.9	2.3
	zk803–97A-3	0.28682	0.03235	0.02266	0.00089	0.10427	0.02334	140.0	9.5	139.9	3.1
	zk803–97A-4	0.21417	0.02040	0.02255	0.00066	0.07825	0.00892	122.7	8.2	139.7	2.9
	zk803–97A-5	0.14788	0.00965	0.02194	0.00037	0.05553	0.00367	140.0	10.4	139.9	2.9
	zk803–97A-6	0.12850	0.00916	0.02191	0.00045	0.04834	0.00383	140.0	15.2	139.9	4.5
	zk803–97A-7	0.16726	0.01184	0.02197	0.00046	0.06272	0.00532	140.0	8.1	139.9	2.6

5.2. Other approaches to determine the timing of intrusion and mineralization

This section discusses the new andradite garnet and titanite U–Pb dating undertaken during this study and uses these data to further constrain the timing of magmatism and mineralization within the study area.

5.2.1. Timing of intrusion

Titanite U–Pb dating has been widely used to constrain the timing of magmatic, hydrothermal, and metamorphic events (Frost et al., 2000; Aleinikoff et al., 2002, 2007; Storey et al., 2006, 2007; Kennedy et al., 2010; Li et al., 2010). However, titanite also typically contains significant amounts of common Pb (Storey et al., 2006, 2007), meaning that the lower intercept age on a Tera–Wasserburg Concordia diagram is generally used to constrain the timing of titanite formation as this intercept does not require a common Pb correction (Tera and Wasserburg, 1972; Aleinikoff et al., 2002; Sun et al., 2012). It is also important to use a matrix-matched external standard for the correction of titanite U–Pb data as using other standards (e.g., a 91500 standard zircon) would almost inevitably yield younger apparent ages (Sun et al., 2012). Our analyses used the OLT-1 titanite standard recommended by Kennedy et al. (2010) for the external standardization of titanite LA–ICP–MS U–Pb data, with the BLR-1 titanite standard used as a monitor during routine analysis. We also employed well-established zircon U–Pb dating procedures for our titanite analyses as these approaches are known to be reliable. All of this means that the titanite LA–ICP–MS U–Pb data obtained during this study should be considered reliable and a precise indicator of the timing of magmatism in the study area.

The titanite analyzed during this study was obtained from fresh samples of the intrusion associated with the Magushan deposit, where titanite is present as an accessory mineral within the porphyritic granodiorite (Fig. 7). This means that the U–Pb age of the titanite analyzed during this study represents the timing of the formation of this intrusion. The titanite yielded a well-defined lower-intercept age of 136.3 ± 2.5 Ma (Fig. 10a) that is within the uncertainty of the zircon U–Pb age for this intrusion. This indicates that the previously obtained zircon U–Pb age for this intrusion is reliable and that the titanite age also documents the timing of the formation of this intrusion.

5.2.2. Timing of mineralization

Garnet contains variable concentrations of U but negligible common Pb and has a high closure temperature for the U–Pb isotope system (>850 °C; Mezger et al., 1989), all of which means it is an ideal geochronometer for the dating of high temperature metamorphism, metasomatism, or hydrothermal activity (Burton and O'Nions, 1992; Vance and Holland, 1993; Burton et al., 1995; Jung and Mezger, 2003). However, the garnet that forms in magmato-hydrothermal environments typically contains a variety of mineral inclusions and therefore may not be ideally suited for U–Pb dating. This issue can be resolved by the use of in situ analytical techniques such as secondary ion mass spectrometry or LA–ICP–MS. The latter enables the simultaneous analysis of both U and Pb isotopes and trace element concentrations (Liu et al., 2010a) but can also be used to remove any effects caused by the

presence of mineral inclusions by targeting inclusion-free areas of garnet, allowing high-quality data acquisition (Deng et al., 2017).

The analysis undertaken during this study yielded a well-defined andradite garnet U–Pb lower intercept age of 135.9 ± 2.7 Ma (Fig. 10b). This age is within uncertainty of the zircon and titanite U–Pb ages for the intrusion within the study area as well as within uncertainty of the molybdenite Re–Os age for the mineralization in this area. This strongly suggests that the formation of the exoskarn andradite garnet in this area is temporally associated with the intrusion of the porphyritic granodiorite. The fact that the timing of exoskarn formation is consistent with the molybdenite Re–Os age obtained for the deposit also suggests that both high temperature skarn and lower temperature mineralizing events in this region were associated with the emplacement of the porphyritic granodiorite (given the different closure temperatures for the garnet U–Pb and molybdenite Re–Os systems). These results strongly suggest that the mineralization in the study area formed during a single phase of magmatic and mineralizing activity as well as supporting the reliability of the molybdenite Re–Os age presented in this study. This conclusion is also consistent with the close spatial (and also likely genetic) relationship between intrusions, orebodies, and alteration in the study area (Figs. 3–5), which is also free of other intrusions and hydrothermal activity.

5.3. Geological significance

5.3.1. Timing of mineralization

The new titanite U–Pb, andradite garnet U–Pb, and molybdenite Re–Os ages presented in this study combined with the previous published zircon U–Pb age for the intrusion in the study area all suggest that the Magushan deposit formed around 136 Ma. The consistency of these ages within uncertainty also suggests that there is a genetic relationship between the intrusion of the porphyritic granodiorite in this area and the formation of the deposit. This indicates that the Magushan deposit formed as a result of a single phase of magmatic activity associated with a single phase of magmato-hydrothermal activity ranging from high-temperature skarn to lower temperature mineralization.

Previous research suggests that magmatism and mineralization in the MLYRMB (except the Ningzhen district) can be split into three main phases (Sun et al., 2003; Mao et al., 2006; Xie et al., 2008, 2011, 2012; Xu et al., 2008; Li et al., 2009, 2019c, 2020a; Yuan et al., 2010; Wang et al., 2015; Liu et al., 2016; Jiang et al., 2017; Zhou et al., 2017). The three phases are (1) 146–135 Ma magmatism in fault-controlled uplifted areas, which is associated with porphyry–skarn Cu–Au deposits; (2) 135–126 Ma magmatism in fault-controlled depressions, which is associated with skarn- and Kiruna-type Fe-oxide apatite deposits, and (3) 126–123 Ma A-type granites within both uplifted areas and depressions that are associated with gold and uranium mineralization. The new data presented in this study provides the first evidence of the timing of the formation of the mineral deposits within the Xuancheng ore district. Previous research reported the ages of mineralization-related intrusive rocks whereas this study directly dated the timing of formation of both mineralization (molybdenite Re–Os) and skarn (andradite garnet U–Pb) in this area (Jiang et al., 2017; Li et al., 2019c, 2020a). These new data provide further evidence of the links between Early Cretaceous magmatism and mineralization within the Xuancheng ore district and the surrounding region. The timing of mineralization documented within this study is also consistent with the timing of the main metallogenic stage of the MLYRMB (Fig. 11), suggesting that the deposits within the Xuancheng ore district formed at the same time as deposits within other districts in this region. This suggests that the deposits within the Xuancheng ore district most likely formed as a result of the same magmatic and mineralizing processes that occurred within other ore districts in the MLYRMB, potentially involving the same sources of magmas and metals and with magmas that underwent the same processes as those associated with ore deposits elsewhere in this region. All of this suggests that the under-explored Xuancheng ore district may be as prospective as the other more mature ore districts within the MLYRMB, and the similarities between these districts mean that exploration techniques used successfully in these other areas may also prove fruitful within the Xuancheng district. This exploration should also focus on the identification of, and exploration around, areas containing Early Cretaceous intrusive rocks given the genetic relationships between this magmatism and the mineralization within this region outlined both here and during previous research.

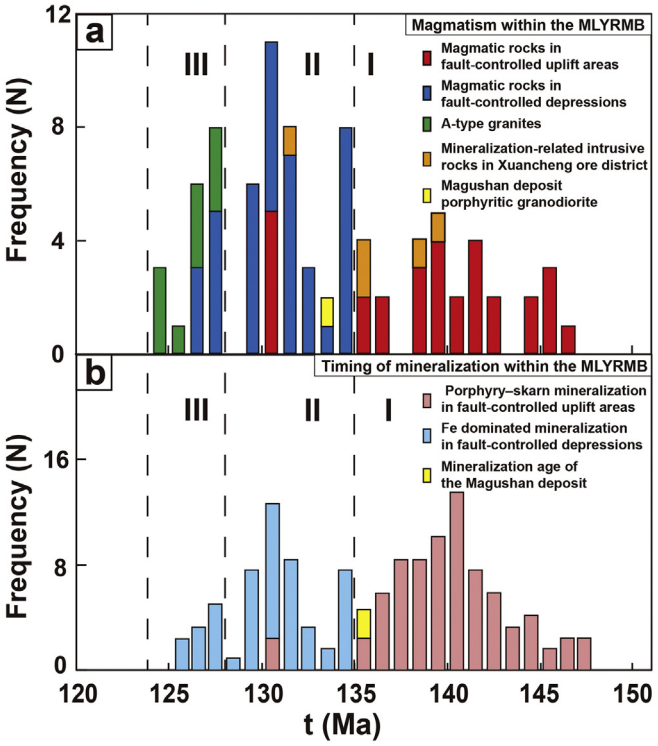

Fig. 11. Histogram showing the timing of formation of magmatic rocks and mineralization within the MLYRMB (data from this study and Sun et al., 2003; Mao et al., 2006; Xie et al., 2008, 2011, 2012; Xu et al., 2008; Li et al., 2009, 2019c, 2020a; Yuan et al., 2010; Wang et al., 2015; Liu et al., 2016; Jiang et al., 2017; Zhou et al., 2017).

5.3.2. Molybdenite Re contents and origin of ore metals

Molybdenite rhenium and osmium data can not only provide evidence of the timing of mineralization using Re–Os isotopic approaches but can also be used to provide evidence of the sourcing of rhenium and by inference other metals within ore deposits (Suzuki et al., 1996). Rhenium concentrations in molybdenite decrease progressively from deposits containing Re (and potentially other metals) derived from the mantle (>100 ppm Re in molybdenite) to those containing metals derived from mixed mantle–crustal sources (tens of ppm of Re in molybdenite) to those containing metals derived from the crust only (<10 ppm Re in molybdenite; Mao et al., 1999). Stein et al. (2001) also suggested that molybdenite from deposits containing metals derived from the mantle generally contain more Re than deposits containing metals derived from the crust, with molybdenite containing very low concentrations of Re (<20 ppm) typically having a metamorphic origin (Stein, 2006).

The molybdenite within the Magushan Cu–Mo skarn deposit contains 21.6–89.7 ppm Re (average of 60.7 ppm; Table 1), suggesting that the deposit contains metals derived from mixed crust–mantle sources. This is consistent with the results of previous research (Li et al., 2020a) into the sourcing and evolution of the mineralization-associated porphyritic granodiorite in this area. This intrusion formed from magmas derived from an enriched region of the lithospheric

mantle that both assimilated upper crustal material and underwent fractional crystallization prior to emplacement, again supporting a link between the magmatism and mineralization within the study area.

5.3.3. The viability and utility of titanite and garnet dating

Recent research (Deng et al., 2017; Seman et al., 2017; Gevedon et al., 2018; Li et al., 2018; Wafforn et al., 2018; Zhang et al., 2018) indicates that garnet U–Pb dating can provide robust constraints on the timing of carbonatite and alkaline magmatism as well as skarn formation. All of these previous studies provide evidence of the reliability of the U–Pb dating of garnet, a finding that is supported by the data presented in this study.

The direct dating of economic mineralization is essential for establishing robust genetic relationships between magmatic and mineralizing, tectonic, and other events as well as for the further refinement of ore deposit models and to further our understanding of the tectonic controls on ore deposit formation within in large metallogenic provinces. Of the currently available radiometric dating methods, the Re–Os method is the only method routinely used to directly date sulfides (Stein et al., 1997, 2001; Selby and Creaser, 2001a; Selby et al., 2002; Ootes et al., 2011; Saintilan et al., 2017a, 2017b, 2018). However, not all mineral deposits contain molybdenite, thus limiting the possible uses of this approach. In addition, the Re–Os dating of other types of sulfides (e.g., pyrite) sometimes yields poor results (Barra et al., 2003; Ying et al., 2014). All of these cases could be supplemented by additional garnet U–Pb dating. Garnet is a common and often voluminous minerals within skarns and is among the earliest mineral to crystallize during skarn formation, meaning that garnet crystallization can accurately capture the timing of the onset of hydrothermal activity (Gevedon et al., 2018) but the low concentrations of U (typically <1 ppm) present in garnet can limit the possible use of garnet U–Pb dating (DeWolf et al., 1996). However, andradite-rich garnet and andradite-rich zones within grossular garnet are both common within the majority of skarns (Meinert et al., 2005) and have the ability to accommodate U as a result of suspected coupled substitutions involving Fe^{3+} (DeWolf et al., 1996; Smith et al., 2004; Guo et al., 2016). This yields a generally positive correlation between increasing mol% andradite values and U concentration, indicating that many skarns are likely to contain garnet with high U concentrations that are suitable for U–Pb analysis. In addition, the timing of skarn formation can be used to examine relationships between skarn mineralization and intrusion in cases involving systems with ambiguous (i.e. multiple possible intrusions) or unknown (i.e. a lack of clear spatial relationships) causative plutons (Gevedon et al., 2018). Garnet U–Pb ages can also be used to provide evidence of multiple stages of magmatism or magmato-hydrothermal activity and could be used to definitively link skarn formation with a distinct phase of magmatism. The closure temperature of the U–Pb system for a 0.5 cm diameter garnet is estimated to exceed 800 °C although no specific estimates for the closure temperature of grossular–andradite garnet have been determined to date (Mezger et al., 1989; Burton et al., 1995; DeWolf et al., 1996). However, skarns typically form at temperatures of 350–650 °C (Bowman, 1998), well below the U–Pb closure temperature of garnet. The low temperature of the formation of garnet in skarn systems combined with these high U–Pb closure temperatures suggests that diffusion is unlikely to affect the results of the U–Pb dating of andradite. This also means that garnet ages can be used to identify multiple phases of skarn formation, as early-formed garnet is unlikely to have their ages reset by later mineralizing events. The trace and rare earth element (REE) concentrations of garnet also provide key information on both skarn formation and the evolution of hydrothermal fluids within skarn systems (e.g., Li et al., 2020b in review).

Titanite U–Pb dating has also been widely used to constrain the timing of magmatic, hydrothermal, and metamorphic events (Frost et al., 2000; Aleinikoff et al., 2002, 2007; Storey et al., 2006, 2007; Kennedy et al., 2010; Li et al., 2010). Titanite is a common accessory mineral in numerous igneous rocks but contains high concentrations of common Pb, meaning that matrix-matched external standards are essential to correct for this and ensure that accurate and precise ages are obtained. In contrast, the zircon U–Pb dating method is relatively simple, one of the reasons it is commonly used for the dating of igneous rocks. This means that titanite U–Pb dating is ideally suited for use in constraining the timing of hydrothermal or mineralizing events rather than determining the age of igneous rocks. This is consistent with the results of previous research (Wanhainen et al., 2005; Li et al., 2010; Deng et al., 2015; Hu et al., 2017; Song et al., 2019) that confirmed the viability of hydrothermal titanite U–Pb dating in determining the timing of hydrothermal activity or mineralization in a range of different areas. The U–Pb dating of titanite by LA–ICP–MS can also simultaneously yield trace and REE concentrations. These data can provide evidence of not just the timing of mineralization but also the evolution of magmato-hydrothermal systems, as evidenced by the research of Xiao et al. (2020) on the Dongguashan porphyry-skarn copper-gold deposit in China.

In summary, garnet and titanite dating methods not only provide reliable geochronological data but also allow further insights into the evolution of hydrothermal and mineralizing systems. These methods may provide the only possible approach to dating a mineralized system that is free of other dateable minerals (e.g., molybdenite) or where the relationship between mineralization and magmatism is unclear. This may be the case in areas with multiple stages of magmatism, within areas containing complexly zoned plutons, or in areas with distal skarn mineralization that has no clear spatial relationship to a pluton.

6. Conclusions

(1) Samples from the Magushan deposit yielded a molybdenite Re–Os age of 137.7 ± 2.5 Ma, an andradite garnet U–Pb age of 135.9 ± 2.7 Ma, and a titanite (accessory mineral within the associated porphyritic granodiorite) U–Pb age of 136.2 ± 2.5 Ma. These data suggest that the deposit formed around 136 Ma.

(2) The Magushan deposit is associated with a single stage of magmatism and associated magmatic-hydrothermal activity, with the formation of the deposit genetically related to the intrusion of the porphyritic granodiorite in this area.

(3) The molybdenite within the deposit has Re contents that are indicative of the sourcing of metals from a mixed mantle-crustal source. This is consistent with the sourcing of the magma that formed the porphyritic granodiorite, which was derived from an enriched region of the lithospheric mantle but assimilated upper crustal material prior to emplacement.

(4) This study provides the first evidence of the timing of mineralization within the Xuancheng ore district of the MLYRMB. These data highlight the prospectivity of this ore district for future mineral exploration and suggests that the Early Cretaceous intrusive rocks in this region should be considered high priority targets for the exploration of skarn-type mineralization.

(5) The U–Pb dating of garnet and titanite can provide reliable geochronological data for constraining the timing of mineralization in areas that lack other dateable minerals (e.g., molybdenite) or where the links between mineralization and magmatism are unclear including areas with multiple stages of magmatism, within areas containing complexly zoned plutons, or in areas with distal skarn mineralization that has no clear spatial relationship to a pluton.

Declaration of Competing Interest

The authors declare that they have no known competing financial interests or personal relationships that could have appeared to influence the work reported in this paper.

Acknowledgements

This research was financially supported by funds from the National Key R&D Program of China (Grant Nos. 2016YFC0600209, 2016YFC0600206), the National Natural Science Foundation of China (Grant No. 41820104007), the Scientific and Technological Program of Land and Resources of Anhui province (Grant No. 2016-K-4) and the China Scholarship Council (Grant No. 201906690036). We thank Tao Lin, Xiansuo Li, Zhi Yang, the Comprehensive Geological Brigade of East China Metallurgical Geographical Prospecting Bureau, and Xuancheng Quanxin Mining Co. Ltd. for assistance and help during the fieldwork and analysis. This manuscript benefited from constructive comments from the editor and two anonymous reviewers.

Appendix A. Supplementary data

Supplementary data to this article can be found online at https://doi.org/10.1016/j.gsf.2020.11.013.

References

Aleinikoff, J.N., Wintsch, R.P., Fanning, C.M., Dorais, M.J., 2002. U–Pb geochronology of zircon and polygenetic titanite from the Glastonbury Complex, Connecticut, USA: an integrated SEM, EMPA, TIMS, and SHRIMP study. Chem. Geol. 188 (1–2), 125–147.

Aleinikoff, J.N., Wintsch, R.P., Tollo, R.P., Unruh, D.M., Fanning, C.M., Schmitz, M.D., 2007. Ages and origins of rocks of the Killingworth dome, south-central Connecticut: implications for the tectonic evolution of southern New England. Am. J. Sci. 307 (1), 63–118.

Barra, F., Ruiz, J., Mathur, R., Titley, S., 2003. A Re–Os study of sulfide minerals from the Bagdad porphyry Cu–Mo deposit, northern Arizona, USA. Mineral. Depos. 38 (5), 585–596.

Bian, Y.C., 1995. On the origin of Magushan Cu–Mo deposit in South Anhui. J. Geol. 19, 17–20 (in Chinese with English abstract).

Bingen, B., Stein, H., 2003. Molybdenite Re–Os dating of biotite dehydration melting in the Rogaland high-temperature granulites, S Norway. Earth Planet. Sci. Lett. 208 (3–4), 181–195.

Bowman, J.R., 1998. Stable-isotope systematic of skarns. In: Lentz, D.R. (Ed.), Mineralized Intrusion-Related Skarn Systems. Mineralogical Association of Canada, Ottawa, Ont, pp. 99–145.

Burton, K.W., O'Nions, R.K., 1992. The timing of mineral growth across a regional metamorphic sequence. Nature 357 (6375), 235–238.

Burton, K.W., Kohn, M.J., Cohen, A.S., O'Nions, R.K., 1995. The relative diffusion of Pb, Nd, Sr and O in garnet. Earth Planet. Sci. Lett. 133 (1–2), 199–211.

Chang, Y.F., Liu, X.P., Wu, C.Y., 1991. The Middle-Lower Yangtze Metallogenic Belt. Geological Publishing House, Beijing (in Chinese with English abstract).

Chen, W., Xu, Z.W., Qiu, W.H., Li, C., Yu, Y., Wang, H., Su, Y., 2015. Petrogenesis of the Yaochong granite and Mo deposit, Western Dabie orogen, eastern-central China: constraints from zircon U–Pb and molybdenite Re–Os ages, whole-rock geochemistry and Sr–Nd–Pb–Hf isotopes. J. Asian Earth Sci. 103, 198–211.

Christensen, J.N., Halliday, A.N., Leigh, K.E., Randell, R.N., Kesler, S.E., 1995. Direct dating of sulfides by Rb–Sr: a critical test using the Polaris Mississippi Valley-type Zn–Pb deposit. Geochim. Cosmochim. Acta 59 (24), 5191–5197.

Deng, X.D., Li, J.W., Zhou, M.F., Zhao, X.F., Yan, D.R., 2015. In-situ LA-ICPMS trace elements and U–Pb analysis of titanite from the Mesozoic Ruanjiawan W–Cu–Mo skarn deposit, Daye district, China. Ore Geol. Rev. 65, 990–1004.

Deng, X.D., Li, J.W., Luo, T., Wang, H.Q., 2017. Dating magmatic and hydrothermal processes using andradite-rich garnet U–Pb geochronometry. Contrib. Mineral. Petrol. 172 (9), 71.

DeWolf, C.P., Zeissler, C.J., Halliday, A.N., Mezger, K., Essene, E.J., 1996. The role of inclusions in U–Pb and Sm–Nd garnet geochronology: Stepwise dissolution experiments and trace uranium mapping by fission track analysis. Geochim. Cosmochim. Acta 60 (1), 121–134.

Du, A.D., Wu, S.Q., Sun, D.Z., Wang, S.X., Qu, W.J., Markey, R., Stein, H., Morgan, J., Malinovskiy, D., 2004. Preparation and certification of Re-Os dating reference materials: molybdenite HLP and JDC. Geostand. Geoanal. Res. 28 (1), 41–52.

Faure, G., 1977. Principles of Isotope Geology. 2nd ed. Wiley, New York.

Frost, B.R., Chamberlain, K.R., Schumacher, J.C., 2000. Sphene (titanite): phase relations and role as a geochronometer. Chem. Geol. 172 (1–2), 131–148.

Fu, Y., Sun, X.M., Li, D.F., Lin, H., 2018. U–Pb geochronology and geochemistry of U-rich garnet from the giant Beiya gold-polymetallic deposit in SW China: constraints on skarn mineralization process. Minerals 8 (4), 128.

Gao, X., Yang, L.Q., Meng, J.Y., Zhang, L.J., 2017. Zircon U–Pb, molybdenite Re–Os geochronology and Sr–Nd–Pb–Hf–O–S isotopic constraints on the genesis of Relin Cu–Mo deposit in Zhongdian, Northwest Yunnan, China. Ore Geol. Rev. 91, 945–962.

Gao, Y., Mao, J.W., Ye, H.S., Li, Y.F., 2018. Origins of ore-forming fluid and material of the quartz–vein type Mo deposits in the East Qinling–Dabie molybdenum belt: a case study of the Qianfanling Mo deposit. J. Geochem. Explor. 185, 52–63.

Gevedon, M., Seman, S., Barnes, J.D., Lackey, J.S., Stockli, D.F., 2018. Unraveling histories of hydrothermal systems via U–Pb laser ablation dating of skarn garnet. Earth Planet. Sci. Lett. 498, 237–246.

Guo, X., Navrotsky, A., Kukkadapu, R.K., Engelhard, M.H., Lanzirotti, A., Newville, M., Ilton, E.S., Sutton, S.R., Xu, H.W., 2016. Structure and thermodynamics of uranium-containing iron garnets. Geochim. Cosmochim. Acta 189, 269–281.

Hong, D.J., Huang, Z.Z., Chan, S.W., Wang, X.H., 2017. Geological characteristics and exploration directions of the Cu–polymetallic ore deposits in the Magushan-Qiaomaishan areas in Xuancheng, Anhui Province. East China Geol. 38, 28–36 (in Chinese with English abstract).

Hu, R.Z., Wei, W.F., Bi, X.W., Peng, J.T., Qi, Y.Q., Wu, L.Y., Chen, Y.W., 2012. Molybdenite Re–Os and muscovite $^{40}Ar/^{39}Ar$ dating of the Xihuashan tungsten deposit, central Nanling district, South China. Lithos 150, 111–118.

Hu, H., Li, J.W., McFarlane, C.R., 2017. Hydrothermal titanite from the Chengchao iron skarn deposit: temporal constraints on iron mineralization, and its potential as a reference material for titanite U–Pb dating. Mineral. Petrol. 111 (4), 593–608.

Jiang, F., Xu, X.C., Qian, S.L., Wang, M., Yang, Q.G., Li, K., 2017. Zircon U–Pb age and genesis of the ore-bearing quartz-dioritic porphyries in the Chating Cu–Au ore deposit, Xuancheng city, Anhui province. Geol. J. China Univ. 23 (4), 591–605 (in Chinese with English abstract).

Jung, S., Mezger, K., 2003. Petrology of basement-dominated terranes: I. Regional metamorphic T–t path from U–Pb monazite and Sm–Nd garnet geochronology (Central Damara orogen, Namibia). Chem. Geol. 198 (3–4), 223–247.

Kennedy, A.K., Kamo, S.L., Nasdala, L., Timms, N.E., 2010. Grenville skarn titanite: potential reference material for SIMS U–Th–Pb analysis. Can. Mineral. 48 (6), 1423–1443.

Leng, C.B., Zhang, X.C., Hu, R.Z., Wang, S.X., Zhong, H., Wang, W.Q., Bi, X.W., 2012. Zircon U–Pb and molybdenite Re–Os geochronology and Sr–Nd–Pb–Hf isotopic constraints on the genesis of the Xuejiping porphyry copper deposit in Zhongdian, Northwest Yunnan, China. J. Asian Earth Sci. 60, 31–48.

Li, J.W., Zhao, X.F., Zhou, M.F., Vasconcelos, P., Ma, C.Q., Deng, X.D., De Souza, Z.S., Zhao, Y.X., Wu, G., 2008. Origin of the Tongshankou porphyry-skarn Cu–Mo deposit, eastern Yangtze craton, Eastern China: geochronological, geochemical, and Sr–Nd–Hf isotopic constraints. Mineral. Deposita 43 (3), 315–336.

Li, J.W., Zhao, X.F., Zhou, M.F., Ma, C.Q., De Souza, Z.S., Vasconcelos, P., 2009. Late Mesozoic magmatism from the Daye region, eastern China: U–Pb ages, petrogenesis, and geodynamic implications. Contrib. Mineral. Petrol. 157 (3), 383–409.

Li, J.W., Deng, X.D., Zhou, M.F., Liu, Y.S., Zhao, X.F., Guo, J.L., 2010. Laser ablation ICP–MS titanite U–Th–Pb dating of hydrothermal ore deposits: a case study of the Tonglushan Cu–Fe–Au skarn deposit, SE Hubei Province, China. Chem. Geol. 270 (1–4), 56–67.

Li, C., Qu, W.J., Du, A.D., Zhou, L.M., 2012. Study on Re–Os isotope in molybdenite containing common Os. Acta Petrol. Sinica 28 (2), 702–708 (in Chinese with English abstract).

Li, D.F., Fu, Y., Sun, X.M., 2018. Onset and duration of Zn–Pb mineralization in the Talate Pb–Zn (–Fe) skarn deposit, NW China: constraints from spessartine U–Pb dating. Gondwana Res. 63, 117–128.

Li, D.F., Tan, C.Y., Miao, F.Y., Liu, Q.F., Zhang, Y., Sun, X.M., 2019a. Initiation of Zn–Pb mineralization in the Pingbao Pb–Zn skarn district, South China: constraints from U–Pb dating of grossular-rich garnet. Ore Geol. Rev. 107, 587–599.

Li, M., Zhang, X., Han, L., Gong, E.P., Wang, G.G., 2019b. The metallogenic setting of the Jiangjiatun Mo deposit, North China: constraints from a combined zircon U–Pb and molybdenite Re–Os isotopic study. Minerals 9 (12), 723.

Li, Y., Yuan, F., Deng, Y.F., Li, X.H., Liu, G.X., Li, H., Lu, S.M., Zhou, Y.Z., 2019c. Origin and metallogenic significance of the ore-forming intrusion and its mafic microgranular enclaves in the Qiaomaishan deposit, Xuancheng city, Anhui province: geochronology, geochemistry, Sr–Nd–Hf–O isotopic constraints. Acta Petrol. Sin. 35 (12), 3838–3862 (in Chinese with English abstract).

Li, Y., Yuan, F., Jowitt, S.M., Deng, Y.F., Hu, X.Y., Liu, G.X., Li, X.H., Zhou, T.F., 2020a. Geochronology, petrogenesis and metallogenic implications of mineralization-related intrusive rocks in the Xuancheng ore district, Eastern China. Ore Geol. Rev. 125, 103690.

Li, Y., Yuan, F., Jowitt, S.M., Deng, Y.F., Hu, X.Y., Zhou, T.F., 2020b. Trace Element Evidence for the Processes Involved in the Formation of Garnet from the Qiaomaishan Cu–W Deposit, Xuancheng Ore District, Anhui Province. Eastern China, Mineralium Deposita (in review).

Liu, X.M., Duan, L.A., 2015. Geological features and metallogenic regularity of the Tongshan-Qiaomaishan Cu–S–W–Fe polymetallic ore deposit in Xuancheng city. Geol. Anhui 25 (3), 174–178 (in Chinese with English abstract).

Liu, Y.S., Gao, S., Hu, Z.C., Gao, C.G., Zong, K.Q., Wang, D.B., 2010a. Continental and oceanic crust recycling-induced melt–peridotite interactions in the Trans-North China Orogen: U–Pb dating, Hf isotopes and trace elements in zircons from mantle xenoliths. J. Petrol. 51 (1–2), 537–571.

Liu, Y.S., Hu, Z.C., Zong, K.Q., Gao, C.G., Gao, S., Xu, J., Chen, H.H., 2010b. Reappraisement and refinement of zircon U–Pb isotope and trace element analyses by LA–ICP–MS. Chin. Sci. Bull. 15, 1535–1546.

Liu, Y., Zhang, R.Q., Matuohuiti, A., Wang, C., Zhang, S.P., Dhen, C.H., Zhang, Z.Y., He, M.Y., Zhang, Y., Yang, X.D., 2016. SHRIMP U–Pb zircon ages, mineral compositions and geochemistry of placer nephrite in the Yurungkash and Karakash rivers deposits, West Kunlun, Xinjiang, Northwest China. Ore Geol. Rev. 72, 699–727.

Luck, J.M., Allègre, C.J., 1982. The study of molybdenites through the $^{187}Re–^{187}Os$ chronometer. Earth Planet. Sci. Lett. 61 (2), 291–296.

Maas, R., McCulloch, M.T., Campbell, I.H., Goad, P.R., 1986. Sm–Nd and Rb–Sr dating of an Archean massive sulfide deposit: Kidd Creek, Ontario. Geology 14 (7), 585–588.

Mao, J.W., Zhang, Z.C., Zhang, Z.H., Du, A.D., 1999. Re–Os isotopic dating of molybdenites in the Xiaoliugou W (Mo) deposit in the northern Qilian mountains and its geological significance. Geochim. Cosmochim. Acta 63 (11−12), 1815–1818.

Mao, J.W., Wang, Y.T., Lehmann, B., Yu, J.J., Du, A.D., Mei, Y.X., Li, Y.F., Zang, W.S., Stein, H.J., Zhou, T.F., 2006. Molybdenite Re–Os and albite $^{40}Ar/^{39}Ar$ dating of Cu–Au–Mo and magnetite porphyry systems in the Yangtze River valley and metallogenic implications. Ore Geol. Rev. 29 (3–4), 307–324.

Mao, J.W., Xie, G.Q., Duan, C., Pirajno, F., Ishiyama, D., Chen, Y.C., 2011. A tectono-genetic model for porphyry–skarn–stratabound Cu–Au–Mo–Fe and magnetite–apatite deposits along the Middle–Lower Yangtze River Valley, Eastern China. Ore Geol. Rev. 43 (1), 294–314.

Mao, J.W., Xiong, B.K., Liu, J., Pirajno, F., Cheng, Y.B., Ye, H.S., Song, S.W., Dai, P., 2017. Molybdenite Re/Os dating, zircon U–Pb age and geochemistry of granitoids in the Yangchuling porphyry W–Mo deposit (Jiangnan tungsten ore belt), China: implications for petrogenesis, mineralization and geodynamic setting. Lithos 286, 35–52.

Markey, R., Stein, H., Morgan, J., 1998. Highly precise Re–Os dating for molybdenite using alkaline fusion and NTIMS. Talanta 45 (5), 935–946.

Mazdab, F.K., 2009. Characterization of flux-grown trace-element-doped titanite using the high-mass-resolution ion microprobe (SHRIMP–RG). Can. Mineral. 47 (4), 813–831.

Meinert, L.D., Dipple, G., Nicolescu, S., 2005. World skarn deposits. Econ. Geol. 100, 299–336.

Mezger, K., Hanson, G.N., Bohlen, S.R., 1989. U–Pb systematics of garnet: dating the growth of garnet in the Late Archean Pikwitonei granulite domain at Cauchon and Natawahunan Lakes, Manitoba, Canada. Contrib. Mineral. Petrol. 101 (2), 136–148.

Mueller, A.G., McNaughton, N.J., 2018. Mineral equilibria and zircon, garnet and titanite U–Pb ages constraining the PTt path of granite-related hydrothermal systems at the Big Bell gold deposit, Western Australia. Mineral. Deposita 53 (1), 105–126.

Nakai, S.I., Halliday, A.N., Kesler, S.E., Jones, H.D., 1990. Rb–Sr dating of sphalerites from Tennessee and the genesis of Mississippi Valley type ore deposits. Nature 346 (6282), 354–357.

Nie, X.T., Sun, J.G., Sun, F.Y., Li, B.L., Zhang, Y.J., Liu, W.Z., 2019. Zircon U–Pb and molybdenite Re–Os dating and geological implications of the Shimadong porphyry molybdenum deposit in eastern Yanbian, northeastern China. Can. J. Earth Sci. 999, 1–17.

Ootes, L., Morelli, R.M., Creaser, R.A., Lentz, D.R., Falck, H., Davis, W.J., 2011. The timing of Yellowknife gold mineralization: a temporal relationship with crustal anatexis? Econ. Geol. 106 (4), 713–720.

Pirajno, F., Zhou, T.F., 2015. Intracontinental porphyry and porphyry-skarn mineral systems in Eastern China: scrutiny of a special case "Made-in-China". Econ. Geol. 110 (3), 603–629.

Qian, S.L., Yang, Q.G., Xie, Z.J., Liu, J., 2017. Geological features and a discussion of ore forming conditions of the Chating porphyry copper (gold) ore deposit in the Xuanzhou district, Anhui Province. Geol. Anhui 27, 81–86 (in Chinese with English abstract).

Saintilan, N.J., Creaser, R.A., Bookstrom, A.A., 2017a. Re–Os systematics and geochemistry of cobaltite (CoAsS) in the Idaho Cobalt belt, Belt-Purcell Basin, USA: evidence for middle Mesoproterozoic sediment-hosted Co–Cu sulfide mineralization with Grenvillian and Cretaceous remobilization. Ore Geol. Rev. 86, 509–525.

Saintilan, N.J., Creaser, R.A., Spry, P.G., Hnatyshin, D., 2017b. Re–Os systematics of LÖllingite and arsenopyrite in granulite-facies garnet rocks: insights into the Metamorphic history and thermal evolution of the broken hill block during the early mesoproterozoic (new South Wales, Australia) Re–Os systematics of LÖllingite-arsenopyrite in Garnetite. Can. Mineral. 55 (1), 29–44.

Saintilan, N.J., Selby, D., Creaser, R.A., Dewaele, S., 2018. Sulphide Re–Os geochronology links orogenesis, salt and Cu–Co ores in the Central African Copperbelt. Sci. Rep. 8 (1), 1–8.

Selby, D., Creaser, R.A., 2001a. Late and mid-Cretaceous mineralization in the northern Canadian Cordillera: constraints from Re–Os molybdenite dates. Econ. Geol. 96 (6), 1461–1467.

Selby, D., Creaser, R.A., 2001b. Re–Os geochronology and systematics in molybdenite from the Endako porphyry molybdenum deposit, British Columbia, Canada. Econ. Geol. 96 (1), 197–204.

Selby, D., Creaser, R.A., 2004. Macroscale NTIMS and microscale LA–MC–ICP–MS Re–Os isotopic analysis of molybdenite: Testing spatial restrictions for reliable Re–Os age determinations, and implications for the decoupling of Re and Os within molybdenite. Geochim. Cosmochim. Acta 68 (19), 3897–3908.

Selby, D., Creaser, R.A., Hart, C.J., Rombach, C.S., Thompson, J.F., Smith, M.T., Bakke, A.A., Goldfarb, R.J., 2002. Absolute timing of sulfide and gold mineralization: a comparison of Re–Os molybdenite and Ar–Ar mica methods from the Tintina Gold Belt, Alaska. Geology 30 (9), 791–794.

Seman, S., Stockli, D.F., McLean, N.M., 2017. U–Pb geochronology of grossular-andradite garnet. Chem. Geol. 460, 106–116.

Shirey, S.B., Walker, R.J., 1995. Carius tube digestion for low-blank rhenium-osmium analysis. Anal. Chem. 67 (13), 2136–2141.

Simonetti, A., Heaman, L.M., Chacko, T., Banerjee, N.R., 2006. In situ petrographic thin section U–Pb dating of zircon, monazite, and titanite using laser ablation–MC–ICP–MS. Int. J. Mass Spectrom. 253 (1–2), 87–97.

Smith, M.P., Henderson, P., Jeffries, T.E.R., Long, J., Williams, C.T., 2004. The rare earth elements and uranium in garnets from the Beinn an Dubhaich Aureole, Skye, Scotland, UK: constraints on processes in a dynamic hydrothermal system. J. Petrol. 45 (3), 457–484.

Smoliar, M.I., Walker, R.J., Morgan, J.W., 1996. Re–Os ages of group IIA, IIIA, IVA, and IVB iron meteorites. Science 271 (5252), 1099–1102.

Song, S.W., Mao, J.W., Xie, G.Q., Chen, L., Santosh, M.S., Chen, G.H., Rao, J.F., Ouyang, Y.P., 2019. In situ LA–ICP–MS U–Pb geochronology and trace element analysis of hydrothermal titanite from the giant Zhuxi W (Cu) skarn deposit, South China. Mineral. Deposita 54 (4), 569–590.

Spencer, C.J., Kirkland, C.L., Taylor, R.J., 2016. Strategies towards statistically robust interpretations of in situ U–Pb zircon geochronology. Geosci. Front. 7 (4), 581–589.

Stein, H.J., 2006. Low-rhenium molybdenite by metamorphism in northern Sweden: recognition, genesis, and global implications. Lithos 87 (3–4), 300–327.

Stein, H.J., Markey, R.J., Morgan, J.W., Du, A., Sun, Y., 1997. Highly precise and accurate Re–Os ages for molybdenite from the East Qinling molybdenum belt, Shaanxi Province, China. Econ. Geol. 92 (7–8), 827–835.

Stein, H.J., Markey, R.J., Morgan, J.W., Hannah, J.L., Scherstén, A., 2001. The remarkable Re–Os chronometer in molybdenite: how and why it works. Terra Nova 13 (6), 479–486.

Storey, C.D., Jeffries, T.E., Smith, M., 2006. Common lead-corrected laser ablation ICP–MS U–Pb systematics and geochronology of titanite. Chem. Geol. 227 (1–2), 37–52.

Storey, C.D., Smith, M.P., Jeffries, T.E., 2007. In situ LA–ICP–MS U–Pb dating of metavolcanics of Norrbotten, Sweden: records of extended geological histories in complex titanite grains. Chem. Geol. 240 (1–2), 163–181.

Sun, W.D., Xie, Z., Chen, J.F., Zhang, X., Chai, Z.F., Du, A.D., Zhao, J.S., Zhang, C.H., Zhou, T.F., 2003. Os–Os dating of copper and molybdenum deposits along the middle and lower reaches of the Yangtze River, China. Econ. Geol. 98 (1), 175–180.

Sun, J.F., Yang, J.H., Wu, F.Y., Xie, L.W., Yang, Y.H., Liu, Z.C., Li, X.H., 2012. In situ U–Pb dating of titanite by LA–ICPMS. Chin. Sci. Bull. 57 (20), 2506–2516.

Suzuki, K., Shimizu, H., Masuda, A., 1996. Re–Os dating of molybdenites from ore deposits in Japan: implication for the closure temperature of the Re–Os system for molybdenite and the cooling history of molybdenum ore deposits. Geochim. Cosmochim. Acta 60 (16), 3151–3159.

Tera, F., Wasserburg, G.J., 1972. U–Th–Pb systematics in three Apollo 14 basalts and the problem of initial Pb in lunar rocks. Earth Planet. Sci. Lett. 14 (3), 281–304.

Vance, D., Holland, T., 1993. A detailed isotopic and petrological study of a single garnet from the Gassetts Schist, Vermont. Contrib. Mineral. Petrol. 114 (1), 101–118.

Wafforn, S., Seman, S., Kyle, J.R., Stockli, D., Leys, C., Sonbait, D., Cloos, M., 2018. Andradite garnet U–Pb geochronology of the Big Gossan skarn, Ertsberg-Grasberg mining district, Indonesia. Econ. Geol. 113 (3), 769–778.

Wan, B., Hegner, E., Zhang, L., Rocholl, A., Chen, Z., Wu, H., Chen, F., 2009. Rb–Sr geochronology of chalcopyrite from the Chehugou porphyry Mo–Cu deposit (Northeast China) and geochemical constraints on the origin of hosting granites. Econ. Geol. 104 (3), 351–363.

Wang, Y.Y., Xiao, Y.L., Yang, X.Y., 2015. Re–Os isotope systematics and fluid inclusions of Xinqiao deposit in Tongling, the Middle-Lower Yangtze River metallogenic belt. Acta Petrol. Sin. 31 (4), 1031–1039 (in Chinese with English abstract).

Wanhainen, C., Billström, K., Martinsson, O., Stein, H., Nordin, R., 2005. 160 Ma of magmatic/hydrothermal and metamorphic activity in the Gällivare area: Re–Os dating of molybdenite and U–Pb dating of titanite from the Aitik Cu–Au–Ag deposit, northern Sweden. Mineral. Deposita 40 (4), 435–447.

Xiao, X., Zhou, T.F., White, N.C., Zhang, L.J., Fan, Y., Chen, X.F., 2020. Multiple generations of titanites and their geochemical characteristics record the magmatic-hydrothermal processes and timing of the Dongguashan porphyry-skarn Cu–Au system, Tongling district, Eastern China. Mineral. Deposita 1–18.

Xie, G.Q., Mao, J.W., Li, R.L., Bierlein, F.P., 2008. Geochemistry and Nd–Sr isotopic studies of Late Mesozoic granitoids in the southeastern Hubei Province, Middle-Lower Yangtze River belt, eastern China: petrogenesis and tectonic setting. Lithos 104 (1–4), 216–230.

Xie, G.Q., Mao, J.W., Zhao, H.J., 2011. Zircon U–Pb geochronological and Hf isotopic constraints on petrogenesis of Late Mesozoic intrusions in the southeast Hubei Province, Middle-Lower Yangtze River belt (MLYRB), East China. Lithos 125 (1–2), 693–710.

Xie, G.Q., Mao, J.W., Zhao, H.J., Duan, C., Yao, L., 2012. Zircon U–Pb and phlogopite ^{40}Ar–^{39}Ar age of the Chengchao and Jinshandian skarn Fe deposits, Southeast Hubei Province, Middle-Lower Yangtze River Valley metallogenic belt, China. Mineral. Deposita 47 (6), 633–652.

Xie, G.Q., Mao, J.W., Bagas, L., Fu, B., Zhang, Z.Y., 2019. Mineralogy and titanite geochronology of the Caojiaba W deposit, Xiangzhong metallogenic province, southern China: implications for a distal reduced skarn W formation. Mineral. Deposita 54, 459–472.

Xu, X.C., Lu, S.M., Xie, Q.Q., Bai, L., Chu, G.Z., 2008. SHRIMP Zircon U–Pb dating for the magmatic rocks in Shizishan ore-field of Tongling, Anhui Province, and its geological implications. Acta Geol. Sin. 82 (4), 500–509 (in Chinese with English abstract).

Xu, X.C., Ji, K., Bai, R.Y., Qian, S.L., Yang, Q.G., Xie, Z.J., 2018. Modes of occurrence of gold and genetic connection between gold and copper in the ores from the Chating porphyry copper-gold deposit, Xuancheng City, Anhui Province. Acta Petrol. Mineral. 4, 575–589 (in Chinese with English abstract).

Yang, J.H., Zhou, X.H., 2001. Rb-Sr, Sm-Nd, and Pb isotope systematics of pyrite: implications for the age and genesis of lode gold deposits. Geology 29 (8), 711–714.

Ying, L.J., Wang, C.H., Tang, J.X., Wang, D.H., Qu, W.J., Li, C., 2014. Re–Os systematics of sulfides (chalcopyrite, bornite, pyrite and pyrrhotite) from the Jiama Cu–Mo deposit of Tibet, China. J. Asian Earth Sci. 79, 497–506.

Yuan, F., Zhou, T.F., Fan, Y., Lu, S.M., Zhang, L.J., Duan, C., Tang, H.M., 2008. Source, evolution and tectonic setting of Mesozoic volcanic rocks in Lozong basin. Anhui Province. Acta Petrol. Sin. 23 (8), 1691–1702 (in Chinese with English abstract).

Yuan, S.D., Hou, K.J., Liu, M., 2010. Timing of mineralization and geodynamic framework of iron-oxide-apatite deposits in Ningwu Cretaceous basin in the Middle-Lower Reaches of the Yangtze River, China: constraints from Ar–Ar dating on phlogopites. Acta Petrol. Sin. 26 (3), 797–808 (in Chinese with English abstract).

Zhai, Y.S., Xiong, Y.L., Yao, S.Z., Lin, X.D., 1996. Metallogeny of copper and iron deposits in the Eastern Yangtse Craton, east-central China. Ore Geol. Rev. 11 (4), 229–248.

Zhang, X., Wang, Y., Leng, C., Zhang, W., Xu, L., Zhu, J., Chen, Y., 2014. Geology, sulfur isotopes and scheelite Sm-Nd age of the Kukaazi Pb-Zn-(Cu-W) polymetallic deposit, Yecheng County, Xinjiang, China. Acta Geol. Sin. (English Ed.) 88 (Supp. 2), 244–246.

Zhang, F.F., Wang, Y.H., Liu, J.J., Wang, J.P., 2015. Zircon U–Pb and molybdenite Re–Os geochronology, Hf isotope analyses, and whole-rock geochemistry of the Donggebi Mo deposit, eastern Tianshan, Northwest China, and their geological significance. Int. Geol. Rev. 57 (4), 446–462.

Zhang, P., Zhao, Y., Kou, L.L., Yang, H.Z., Yang, F.C., 2016. Zircon U–Pb and molybdenite Re–Os geochronology of copper–molybdenum deposits in southeast Liaoning Province, China. Int. Geol. Rev. 58 (12), 1481–1491.

Zhang, Y., Shao, Y.J., Zhang, R.Q., Li, D.F., Liu, Z.F., Chen, H.Y., 2018. Dating ore deposit using garnet U–Pb geochronology: example from the xinqiao Cu–S–Fe–Au deposit, Eastern China. Minerals 8 (1), 31.

Zhang, S.T., Chen, H.Y., Shu, Q.H., Zhang, Y., Chu, G.B., Cheng, J.M., Tian, J., 2019. Unveiling growth histories of multi-generational garnet in a single skarn deposit via newly-developed LA–ICP–MS U–Pb dating of grandite. Gondwana Res. 73, 65–76.

Zhou, T.F., Fan, Y., Yuan, F., Zhang, L.J., Qiao, B., Ma, L., Yang, X.F., Cooke, D.R., 2011. Geochronology and significance of volcanic rocks in the Ning-Wu Basin of China. Sci. China Earth Sci. 54 (2), 185–196.

Zhou, T.F., Wang, S.W., Fan, Y., Zhang, D.Y., White, N.C., 2015. A review of the intracontinental porphyry deposits in the Middle-Lower Yangtze River Valley metallogenic belt, Eastern China. Ore Geol. Rev. 65 (1), 433–456.

Zhou, T.F., Fan, Y., Wang, S.W., White, N.C., 2017. Metallogenic regularity and metallogenic model of the Middle-Lower Yangtze River Valley Metallogenic Belt. Acta Petrol. Sin. 33 (11), 3353–3372 (in Chinese with English abstract).